Renormalization of quenched randomness in Biot theory

Eric Smith
Applied Research Laboratories, The University of Texas at Austin, Austin, Texas 78731
(Received 21 January 2000; revised manuscript received 28 March 2001; published 29 August 2001)

This is the first of two papers that develop a theory of perturbative acoustic scattering and localization in fluid-saturated porous solids. The Biot effective-medium theory is used as the general model of porous-medium acoustics, and replica field functional integrals are introduced to incorporate spatially δ-function correlated fluctuations of the Biot parameters. This paper develops the renormalization group and frequency-dependent definition of the effective medium in the limit of inviscid saturating fluid. (Generalized) density fluctuations are found to create an RG-relevant effective coupling, which renormalizes to a universal form in an asymptotic limit of large flow range. A scattering-induced dispersion is also identified, which, in a simple example assuming superfluid helium as saturant, serves as an experimental probe of heterogeneity in the Biot tortuosity parameter.

DOI: 10.1103/PhysRevB.64.134202 PACS number(s): 63.50.+x, 61.43.Gt, 62.30.+d, 61.43.−j

I. INTRODUCTION: SCATTERING IN POROUS-MEDIUM ACOUSTICS

Continuum mechanics provides a natural and intuitive description of a great many fluids and solids, because their atomic or molecular granularity is not resolved by commonly achievable wavelengths. The linear acoustics and elasticity of such materials is often describable at leading order by Helmholtz equations with homogeneous parameters, and it is well understood how to compute scattering from local fluctuations in these parameters perturbatively. When techniques such as the renormalization group (RG) are used to organize the leading asymptotics of large perturbative orders,[1] it can be found that coherence effects cause dispersion, and that the aggregation of multiple scattering can be considerably stronger or weaker than would be expected by naive summation of Born-approximation cross sections. A surprising consequence of this is the possibility of acoustic localization,[2–4] whereby solutions to the Helmholtz equation are transformed from extended traveling waves to modes spatially confined by coherent backscatter.

The acoustics of fluid-saturated porous solids also has a continuum description, known as Biot theory.[5,6] It directly generalizes linear elasticity to the symmetries of interpenetrating, independent, fluid and solid deformational degrees of freedom, and all of its salient predictions have been quantitatively confirmed in experiments. Biot theory is often used to describe granular solids with macroscopic grain sizes, for which it is easy to produce acoustic wavelengths from many down to one times the grain or pore diameters. As increasing frequency successively resolves heterogeneities in grain arrangements and ultimately individual grain boundaries, it is clear that homogeneous Biot theory must continue to some strong multiple-scattering theory, but not even a perturbative theory of porous-medium acoustic scattering analogous to the elastic case has yet been developed. Consequently, the relation of multiple to Born-approximation scattering strengths, and the possibility of acoustic localization, have not been studied for porous media at all.

This is the first of two papers on acoustic scattering in heterogeneous porous media, where the heterogeneities are described by parameter fluctuations about a homogeneous Biot-theory background. Its concern is RG organization of arbitrary-order perturbative effects, and the definition of frequency-dependent effective medium parameters and scattering operators. A companion paper[7] will use these results to study acoustic localization in porous media, and in particular the differences from elastic localization that arise from Biot theory's richer spectrum of wave types.

A. The universality of Biot theory

The theory developed here is the first step in the continuation from homogeneous Biot theory toward a grain-scale description of strong multiple scattering. It can be carried out entirely within a Biot framework because Biot theory is a complete effective field theory (EFT) in the sense of Weinberg:[8] Its conservative sector, at lowest order in derivatives, is the most general form following from analyticity and the symmetries of co-present liquid and solid degrees of freedom.[9] In other words, if the mean properties of any porous medium have an approximate Biot description at some frequency, arbitrary small alterations in the medium composition or arrangement can be represented by fluctuations in some combinations of the Biot parameters.

A description of heterogeneous porous media based on renormalized Biot theory is appealing for two reasons. First, it incorporates frequency dependence into the Biot effective medium in a logically consistent way. The constitutive relations of Biot theory[10] (discussed in more detail below) are usually derived by homogenization[9,11] or volume averaging,[12] either of which assumes a large separation of scales between wavelength and grain or pore diameters. Yet for many frequencies of interest to resolve statistical fluctuations in grain or pore configuration, a homogenization volume is not cleanly defined. If instead the effective medium is assumed defined by its symmetries, the RG can be used to relate dispersion or frequency-dependent scattering strength to the magnitude and scale of effective parameter fluctuations, whose low-frequency average corresponds to the homogenization result.

Second, keeping explicit the ''most general form consistent with the symmetries''[8] embeds homogeneous Biot theory as the lowest nontrivial order in a spatial and temporal derivative expansion, and provides classical scaling estimates for when the coefficients of higher derivatives become important. In principle, it is by successive inclusion of these higher-order derivatives that one performs the complete continuation to the theory that resolves individual grains.

Even without going beyond the linear wave equation, though, the RG can have interesting consequences. Precisely because it is a complete EFT, Biot theory is generally expected to be the *universal* description of homogenized porous media.[9] The possibility of coherent backscatter and localization at strong coupling, however, suggest *phase transitions* from the Biot effective medium into something which has no analog in acoustic or elastic theory. The features of such a localization transition will be discussed in detail in the companion paper.

The universal nature of Biot theory is thus important in two respects. First, it shows that Biot-parameter perturbation theory is not only well-defined but *generic* as a long-wavelength description of porous-medium heterogeneity. Second, the only way one expects it to be violated at the order of the Helmholtz equation is by a phase transition, as may be induced by localization.

B. Goals of this work

One purpose of the present paper is to show how to compute and organize arbitrary orders of perturbative acoustic scattering from spatially delta-function correlated fluctuations in porous-medium properties. No such general formulation currently exists, but there is a natural way to create one by extending the replica-field representation of quenched randomness already applied successfully to acoustic and elastic media.[3] Replica acoustics provides a single, coherent framework for organizing all-orders perturbative scattering,[13] and perturbative[3] and nonperturbative[4] descriptions of localization. However, it provides no way to incorporate intrinsic dissipation (due to its reliance on analyticity), and this requires that all derivations assume ideal fluids.

A second purpose is to derive dispersion and enhanced-scattering effects that can be used to estimate the internal heterogeneity of porous solids experimentally. If superfluid helium is used as a saturant, the inviscid calculations in this and the next paper can be applied directly to laboratory experiments. The strongly temperature-dependent viscosity of liquid helium has already been used[14] to measure bulk-averaged properties of the dynamic tortuosity of the pore space, through a boundary-layer dispersion mechanism[15] similar to one first derived by Biot.[5] The present paper derives a scattering-induced dispersion in the inviscid limit, which may be used to estimate the fluctuations of local tortuosity around the mean value.

It is also a well-understood property of (homogeneous) porous-medium acoustics that fluid-driven dissipation and dispersion have qualitatively distinct low-frequency and high-frequency forms, between which a transition occurs when the fluid's viscous boundary layer thickness is comparable to a characteristic pore radius.[15,16] Therefore, scattering signatures derived here for inviscid fluids may persist for nonideal fluids at sufficiently high frequencies, though the relation is not quantitatively developed in these papers.

A third, explicit object of the RG flow in this paper is the wavelength-scale effective theory, a necessary input for localization calculations in the companion paper. It will be found that the porous-medium RG asymptotically collapses a large range of small-scale heterogeneities onto a single form of the long-wavelength effective scattering operator, and in this regard porous-medium localization is qualitatively richer than its elastic counterpart.

In the elastic problem, a single, scalar source of scattering (density perturbations) could be assumed without loss of generality,[3] and whether it was defined at a microscopic or wavelength scale was indifferent up to specification of the scattering strength. Yet in forming the sigma model to describe localization, it is explicitly the scattering vertex and density of states at the physical pole that determines the initial coupling strength (see Ref. 3 for the role of on-shell scattering). The asymptotic form of the porous-medium scattering operator couples very differently to different Biot wave types, and this is the origin of qualitative differences between Biot and elastic localizing transitions.

The parameter space for Biot backgrounds and potential scattering operators is extremely large, so the universal characteristics of the Biot RG will be emphasized for the formal simplicity they provide, specifically the ability to identify a preferred type of localizing transition. In the practical examples treated quantitatively, it will turn out that strong coupling and the breakdown of perturbation theory are often encountered before this asymptotic regime is reached, so the degree of simplification provided by universal asymptotics in a given application is unclear. On the other hand, in the same examples, the most natural sources of scattering are near the asymptotic forms even before renormalization, so the ''universal'' results remain appropriate.

C. Organization and audience

It is expected that some elements of this work will be unfamiliar to readers in either the porous-medium acoustics or replica-field/localization audiences. Because every aspect of the inviscid quenched-random scattering problem in porous media directly extends the form for linear elasticity, the replica methods commonly used to treat acoustic localization will be followed closely. Since Biot theory is usually applied at the level of classical wave equations, the first step in this construction will be to recast these in a variational form amenable to replica treatment. Notation will be chosen so that matrix-valued Biot parameters naturally generalize the Lamé parameters of elasticity, and the rest of the replica construction in terms of these will be as in Refs. 3, 4, and 13.

Important features of Biot theory that may be unfamiliar to localization audiences are the spectrum and properties of its wave types, and the constitutive relations between its matrix-valued Lamé parameters and the densities and moduli most readily measured in the laboratory. Therefore, Sec. II,

which gives the defining relations, will open with a brief summary of the phenomenology of homogeneous Biot theory.

Section II then proceeds with the variational construction, the definition of Biot Green's functions in terms of functional integrals, and the replica average over background fluctuations. Section III organizes the naive power counting and perturbation theory of the RG for the compressional sector, as a starting point. It shows that only density fluctuations are classically relevant, and introduces graphs for the vertices involving only longitudinal excitations. Section IV derives the perturbative RG corrections in this naive version of the so-called ''poroacoustic'' sector,[17] in which transverse waves are simply ignored. Section V analyzes the RG flow for fixed points. Since flow is toward strong coupling, there are no fixed points as in the example of Ref. 1. There are, however, *stationary rays*, representing fixed forms of the interaction vertex, which are studied for the flow of their one-parameter coupling.

A powerful consequence of assembling the Biot parameters into 2×2 matrices is that the wave equations they induce have an intuitive geometric interpretation, which appears not to have been presented before, and is developed in Sec. VI. These matrix-valued equations have a simple three-dimensional vector structure, from which all of the main features of Biot theory described in Sec. II become immediately apparent. Though it is hoped that this description will render Biot theory simple and intuitive, its primary purpose is to enable conclusions about the universal features of renormalization corrections, independent of detailed specification of initial conditions of the RG flow.

Section VII examines a limited class of shear wave effects. First the naive poroacoustic limit is related to the more complicated treatment of the limit of vanishing shear modulus. Then, the degenerate, finite shear modulus is considered. The complicated nature of scattering into shear excitations in this problem seems to preclude a unified treatment of the various approximate limits just listed. Therefore, two examples are elaborated in Sec. VIII, both to show how the disjoint pieces fit together and to give a laboratory example where dispersion provides an estimate for heterogeneity. This section contains the ''experimental applications'' of the paper. Finally, Sec. IX closes with conclusions and implications.

II. BIOT THEORY AND REPLICA FIELDS

A. The Biot spectrum and constitutive relations

Biot's effective-medium theory of the acoustics of fluid-saturated porous solids has two essential components. The first is a prediction of three wave types based entirely on the symmetries of homogeneous, interpenetrating, independent fluid and solid deformation degrees of freedom.[5,6] The second is a set of constitutive relations between the parameters in a given Biot model and the various elastic moduli and densities that characterize the solid frame and saturating fluid.[10]

Biot theory predicts the existence of two independent compressional waves and one shear wave. The first compressional wave, or ''fast wave,'' propagates in-phase compression and displacement of the fluid and solid, and has the fastest wave speed in the medium. The second compressional wave, or ''slow wave,'' propagates out-of-phase compression and displacement of fluid and solid, and has a slower speed. In both the fast wave (unless a special matching condition is fine tuned by choice of materials) and the slow wave (always), there is local fluid motion relative to the solid, and for viscous fluids this results in an intrinsic dissipation and dispersion. For many common combinations of nonideal fluids and solids, the fast wave dissipation is small, but the slow wave dissipation can be so large that the wave is essentially diffusive.[18] Because dissipation in shearing fluid boundary layers is always higher than in bulk fluid compression, the saturant viscosity is generally a more important factor for either Biot compressional wave than for simple acoustics in the same fluid. The Biot shear wave is a straightforward generalization of the elastic shear wave, only having enhanced dissipation for nonideal fluids, due again to relative fluid/solid displacements. The existence of all three wave types relies on consolidation of the porous solid frame,[19] which in general results in two different bulk compressional moduli for the frame and the elastic solid (say, grain material) of which it is composed.

All three Biot waves have been observed in laboratory experiments, with both viscous (water) (Ref. 19) and near-ideal (superfluid helium) (Ref. 14) saturating fluids. Wave speeds predicted from independent measurements of solid frame and fluid properties have shown excellent quantitative fits to experiment, when one internal pore property (dynamic tortuosity) is unknown,[14,19] and in comparisons using two fluids (water and liquid helium), fits obtained with one fluid yield predictions for the other fluid that match data with no adjustable parameters.[14,20]

To understand the constitutive relations of Biot theory, it is necessary first to define its deformational degrees of freedom. Following the notation of Stoll,[16,21] the locally volume averaged displacement of the solid from a reference rest position is denoted u. The corresponding averaged fluid displacement is called U. The porosity β of the frame is the average fraction of any macroscopic enclosed volume which is pore space. It is generally convenient to work with the volume-weighted displacement of the fluid relative to the solid, denoted $w\equiv\beta(u-U)$.

The derivation below will be carried out in general spatial dimension d, for reference to similar problems,[1,2,13] though $d=3$ will be used in evaluation of some final quantities. Spatial indices for vectors and gradients will be denoted $u,w,\nabla=[u^i,w^i,\nabla^i]_{i=1,\ldots,d}$, spatial differentiation denoted by a comma where this simplifies notation, and the summation convention adopted for repeated indices.

A strain tensor is defined, to linear order in derivatives, for each displacement field,

$$\epsilon^{ij}\equiv\tfrac{1}{2}(u^{i,j}+u^{j,i}), \tag{1}$$

$$\varepsilon^{ij}\equiv\tfrac{1}{2}(w^{i,j}+w^{j,i}), \tag{2}$$

and the traces of the strain tensors are denoted

$$e \equiv \nabla \cdot u = \mathrm{Tr}(\epsilon) \equiv \epsilon^{ii}, \tag{3}$$

$$\zeta \equiv \nabla \cdot w = \mathrm{Tr}(\varepsilon) \equiv \varepsilon^{ii}. \tag{4}$$

ζ is the so-called ''increment of fluid content.''[6,16]

In homogeneous systems, the equations relating stress gradients to accelerations of u and w are, with $\partial_t(\ ) \equiv (\dot{\ })$,

$$\rho \ddot{u}^i - \rho_f \ddot{w}^i = \nabla^i [(H-2\mu)e - C\zeta] + \nabla^j (2\mu \epsilon^{ij}), \tag{5}$$

$$\rho_f \ddot{u}^i - m\ddot{w}^i = \nabla^i [Ce - M\zeta]. \tag{6}$$

The parameters ρ, ρ_f, m, H, C, M, and μ are a natural set for defining Biot theory variationally, for reasons to be explained below. On the other hand, the natural densities to measure in the laboratory are ρ_r of the solid grain material (r for ''rock'') and ρ_f of the fluid. An additional parameter α_∞ is needed to fix the independent coefficient m. α_∞ is the high-frequency, real-valued limit of a complex-valued dynamic tortuosity (in the frequency domain), which also accounts for the interaction of pore walls and viscous boundary layers, and can be derived from electrical conductivity measurements and fluid viscosity. In terms of these,[18]

$$\rho \equiv (1-\beta)\rho_r + \beta \rho_f \tag{7}$$

is the mean density of the system, and

$$m \equiv \frac{\alpha_\infty \rho_f}{\beta}. \tag{8}$$

The two familiar moduli to measure are the bulk modulus K_r of the homogeneous frame material (the ''grains'') and K_f of the fluid. A different bulk modulus, K_b, is defined by compression of the free-draining frame, and μ is the corresponding frame shear modulus.[16] In terms of these, the moduli in Eqs. (5) and (6) are defined by[18]

$$D \equiv K_r [(1-\beta) + \beta K_r / K_f] \tag{9}$$

(a convenient aggregate), and

$$H \equiv K_b + \frac{4}{3}\mu + \frac{(K_r - K_b)^2}{D - K_b}, \tag{10}$$

$$C \equiv \frac{K_r (K_r - k_b)}{D - K_b}, \tag{11}$$

and

$$M \equiv \frac{K_r^2}{D - K_b}. \tag{12}$$

A useful rule of thumb for the examples treated below is that the speed of the Biot slow wave is controlled by whichever of the fluid or solid-frame is more compressible. Since the frame compressional and shear modulus are typically similar, in the latter case the slow and shear speeds will have comparable order of magnitude, while in the former, the fast and shear waves will be more similar.

B. Variational formulation

The correspondence between Eqs. (5) and (6) and linear elasticity becomes transparent when the density parameters are assembled into a matrix

$$[\rho] \equiv \begin{bmatrix} \rho & -\rho_f \\ -\rho_f & m \end{bmatrix}, \tag{13}$$

and H, C, M into a matrix generalizing the scalar bulk modulus:

$$[K] \equiv \begin{bmatrix} H & -C \\ -C & M \end{bmatrix}. \tag{14}$$

The shear modulus is the only parameter in a matrix generalization

$$[\mu] \equiv \begin{bmatrix} \mu & 0 \\ 0 & 0 \end{bmatrix}, \tag{15}$$

and in terms of these the Lamé parameter λ generalizes to

$$[\lambda] \equiv [K] - 2[\mu]. \tag{16}$$

$[\rho]$, like its scalar counterpart, relates velocities $\dot{u}$ and $\dot{w}$ to their conjugate momenta, from which it is straightforward to define the kinetic energy. Similarly, $[\lambda]$ relates pressures to dilational strains, and $[\mu]$ shear stress to shear strain, from which the stress energy follows by integration. Equations (5) and (6) are thus naturally obtained by variation of the action functional

$$S = \int dt \int d^d x \left\{ \frac{1}{2} \begin{bmatrix} \dot{u} & \dot{w} \end{bmatrix}^i [\rho] \begin{bmatrix} \dot{u} \\ \dot{w} \end{bmatrix}^i - \frac{1}{2} \begin{bmatrix} e & \zeta \end{bmatrix} [\lambda] \begin{bmatrix} e \\ \zeta \end{bmatrix} - \mu(\epsilon^{ij}\epsilon^{ij}) \right\}, \tag{17}$$

in which two dimensional matrix multiplication is indicated by juxtaposition of matrices, row and column vectors.

The sense in which the Biot parameters of Eqs. (5) and (6) are natural is now apparent: Matrix $[\mu]$ of Eq. (15) identifies uniquely the degree of freedom supporting a shear stress, and the Biot displacements and parameters are chosen to respect this diagonalization. The remaining freedom in the admixture of u and U in w is fixed by making ρ_f the fluid inertia parameter in Eq. (5), and thus the off-diagonal density coordinate. This symmetry-based definition, which applies equally to the renormalized effective theory at any scale, is actually more fundamental than the constitutive relations of the last section. This will be seen in Sec. VII when scattering induces entrainment of part of the fluid with the frame, leading to a frequency-dependent rotation of the effective degrees of freedom away from the definitions obtained from zero-frequency homogenization.

The action (17), when used with piecewise continuous parameters, produces the conventional interface conditions for permeable boundaries.[22] When the parameters are given arbitrary, δ-function correlated fluctuations below, it will

produce the corresponding continuity conditions as scattering perturbations to the homogeneous equations of motion.

The notion of δ-function parameter fluctuations, like that of locally defined fields u, w, is of necessity band limited, and there will be some fundamental length l_0, called the *natural scale*, such that wave number components $\gtrsim 2\pi/l_0 \equiv \Lambda_0$ are considered excluded from Fourier transforms of fields and parameters. For granular media, l_0 is typically expected to be one to several times a grain or pore diameter, and the description in which all wave numbers up to Λ_0 define ''local'' excitations is called the bare theory.

A final simplification in Biot media, as in linear elasticity, will be to work not with the displacement fields themselves, but with their scalar and vector potentials. ρ_f and l_0 will be used to give these dimensions that simplify notation in what follows. Potentials are defined by the relations

$$u \equiv \sqrt{\rho_f} l_0^{(d/2+1)} (\nabla \phi_R + \nabla \times A_R), \tag{18}$$

$$w \equiv \sqrt{\rho_f} l_0^{(d/2+1)} (\nabla \varphi_R + \nabla \times a_R), \tag{19}$$

where in components $(\nabla \times A_R)^i \equiv \epsilon^{ijk} A_R^{k,j}$, $(\nabla \times a_R)^i \equiv \epsilon^{ijk} a_R^{k,j}$, and ϵ^{ijk} is the totally antisymmetric symbol. The shear potential need not be gauged (though that is certainly admissible) to remove the longitudinal component, because this automatically decouples from all physical quantities.

C. Green's functions, statistics, and replicas

The regular properties of acoustic propagation in randomly heterogeneous media are captured by the dyadic of Green's functions between components i and j of either displacement field, averaged over statistical variations of the densities and moduli. For homogeneous media, individual components of this dyadic have been computed in a variety of cases. Far-field solutions for sources coupling only to the solid frame were considered in Ref. 23. Solutions with constant modulus and dissipation parameters in $d=3$ (Ref. 24) and general frequency dependence in $d=2$ (Ref. 25) were subsequently computed. (Reference 25 also gives a method whereby thermoelastic solutions, already computed in $d=3$,[26] may be mapped to Biot problems.)

In all of these, the response to a point force in either the fluid or solid was considered, and closed-form spatial solutions sought. Below, since all scattering operators follow directly from parameter variations in the action (17), symmetric Green's functions of displacement potentials will be more useful in expanding perturbation theory. Further, the renormalization group is most easily implemented for this problem in wave number variables. In the inviscid limit, these simplifications will admit compact, closed-form solutions that immediately generalize those of conservative elasticity.

Green's functions in a single parameter realization will be denoted as expectation values (for reasons to become apparent shortly). It is most convenient to convert time-domain correlations to the the frequency domain, as

$$[\mathcal{G}^{ij}(t',x';t,x)] \equiv \left\langle \begin{bmatrix} u \\ w \end{bmatrix}^i_{t',x'} \begin{bmatrix} u & w \end{bmatrix}^j_{t,x} \right\rangle \equiv \int \frac{d\omega'}{2\pi} \int \frac{d\omega}{2\pi} e^{-i(\omega' t' - \omega t)} \left\langle \begin{bmatrix} u \\ w \end{bmatrix}^i_{-\omega',x'} \begin{bmatrix} u & w \end{bmatrix}^j_{\omega,x} \right\rangle \tag{20}$$

(note that $u_{\omega,x}$ has dimensions of length$\times$time).

Because backgrounds are time-independent, frequency Green's functions have the form

$$\left\langle \begin{bmatrix} u \\ w \end{bmatrix}^i_{-\omega',x'} \begin{bmatrix} u & w \end{bmatrix}^j_{\omega,x} \right\rangle \equiv \frac{c_0}{l_0} 2\pi \delta(\omega' - \omega) \left\langle \begin{bmatrix} u \\ w \end{bmatrix}^i_{x'} \begin{bmatrix} u & w \end{bmatrix}^j_{x} \right\rangle_{\omega}. \tag{21}$$

A reference speed c_0 has been inserted, to preserve the dimensions of fields in the correlation. As Dirac δ functions are expected to become Kronecker δ's of domains of order l_0, finite time resolution is expected to place $c_0 \sim c_f$ (fluid speed), or whatever speed characterizes transmission of information across such a domain. (Nothing below depends on the choice of c_0.)

Green's functions for equations of motion (5) and (6) may be obtained directly from the Lagrangian in Eq. (17) by defining weight function

$$Z \equiv \int \mathcal{D}\phi_R \mathcal{D}\varphi_R \mathcal{D}A_R \mathcal{D}a_R e^{-L}, \tag{22}$$

and evaluating the Gaussian integral

$$\left\langle \begin{bmatrix} u \\ w \end{bmatrix}^i_{x'} \begin{bmatrix} u & w \end{bmatrix}^j_{x} \right\rangle_{\omega} = \frac{1}{Z} \int \mathcal{D}\phi_R \mathcal{D}\varphi_R \mathcal{D}A_R \mathcal{D}a_R e^{-L} \begin{bmatrix} u \\ w \end{bmatrix}^i_{x'} \begin{bmatrix} u & w \end{bmatrix}^j_{x} \tag{23}$$

(which motivates the notation as expectation values). The fluctuations replace the dyadic in Eq. (23) with the operator inverse of the wave equation kernel. Nondimensionalized, the Lagrangian in Eqs. (22) and (23) is

$$L=\frac{1}{\rho_f l_0^{(d+2)}}\int d^dx\left\{\frac{1}{2}\omega^2[u \quad w]^i[\rho]\begin{bmatrix}u\\w\end{bmatrix}^i-\frac{1}{2}[e \quad \zeta][\lambda]\begin{bmatrix}e\\\zeta\end{bmatrix}-\mu(\epsilon^{ij}\epsilon^{ij})\right\}. \tag{24}$$

Equation (23) is not directly suitable for averaging over backgrounds, because the Green's function is not itself a functional integral. This problem is overcome with the replica-field trick,[27] which begins with the observation that Eq. (23) may trivially be written

$$\left\langle\begin{bmatrix}u\\w\end{bmatrix}^i_{x'}[u \quad w]^j_x\right\rangle_\omega=\lim_{n\to 0}Z^{n-1}\int \mathcal{D}\phi_R\mathcal{D}\varphi_R\mathcal{D}A_R\mathcal{D}a_R e^{-L}\begin{bmatrix}u\\w\end{bmatrix}^i_{x'}[u \quad w]^j_x. \tag{25}$$

The argument of the limit may be obtained at integer n by promoting each spatial displacement field to a vector of n *replicas*: $u^i\to[u^i_\mu]_{\mu=1,\ldots,n}$, $w^i\to[w^i_\mu]_{\mu=1,\ldots,n}$. Biot matrix products go to replica sums,

$$[u \quad w]^i[\rho]\begin{bmatrix}u\\w\end{bmatrix}^i\to[u \quad w]^i_\mu[\rho]\begin{bmatrix}u\\w\end{bmatrix}^i_\mu, \tag{26}$$

in which the replica index will be left implicit below, to avoid overloading notation. In fluctuation integrals, the symbols u^i and w^i will also continue to be used, but will now represent whole replica vectors except where explicitly indexed. For n independent displacement fields, the weight function $Z\to Z^n$. If one computes only Green's functions of a single (say the $\mu=1$) component, one factor of Z contributes the numerator in Eq. (23), and the other $n-1$ components remain untouched, leaving the same formal limit as Eq. (25):

$$\left\langle\begin{bmatrix}u\\w\end{bmatrix}^i_{x'}[u \quad w]^j_x\right\rangle_\omega=\lim_{n\to 0}\int \mathcal{D}\phi_R\mathcal{D}\varphi_R\mathcal{D}A_R\mathcal{D}a_R e^{-L}\begin{bmatrix}u\\w\end{bmatrix}^i_{(1),x'}[u \quad w]^j_{(1),x}. \tag{27}$$

It is now possible to decompose the densities and moduli into mean and variable parts, $[\rho]=[\rho_0]+[\rho']$, $[\lambda]=[\lambda_0]+[\lambda']$, $[\mu]=[\mu_0]+[\mu']$, and evaluate the averaged Green's function as the limit of a single functional integral. Another weight function is introduced to normalize the measure over background fluctuations,

$$\mathcal{Z}\equiv\int \mathcal{D}\rho'\mathcal{D}\lambda'\mathcal{D}\mu' e^{-L^{\text{weight}}[\rho',\lambda',\mu']}, \tag{28}$$

and the statistically averaged Green's function, denoted with an overbar, is defined as

$$\overline{\left\langle\begin{bmatrix}u\\w\end{bmatrix}^i_{x'}[u \quad w]^j_x\right\rangle_\omega}\equiv\frac{1}{\mathcal{Z}}\int \mathcal{D}\rho'\mathcal{D}\lambda'\mathcal{D}\mu' e^{-L^{\text{weight}}[\rho',\lambda',\mu']}\left\langle\begin{bmatrix}u\\w\end{bmatrix}^i_{x'}[u \quad w]^j_x\right\rangle_\omega, \tag{29}$$

where the replica form (27) is to be used on the right-hand side, and the $n\to 0$ limit is taken *after* evaluation of the background integral.

Transforming from position to wave number representation of fields, and suppressing the subscript ω from now on,

$$\overline{\left\langle\begin{bmatrix}u\\w\end{bmatrix}^i_{x'}[u \quad w]^j_x\right\rangle_\omega}\equiv\int\frac{d^dk'}{(2\pi)^d}\int\frac{d^dk}{(2\pi)^d}e^{i(-k\cdot x+k'\cdot x')}\overline{\left\langle\begin{bmatrix}u\\w\end{bmatrix}^i_{-k'}[u \quad w]^j_k\right\rangle}. \tag{30}$$

The free action, which has constant coefficients $[\rho_0]$, $[\lambda_0]$, $[\mu_0]$, diagonalizes simply in terms of compressional and shear potentials:

$$L^{\text{free}}=\frac{1}{2}\int\frac{d^dk}{(2\pi)^d}\left\{[\phi_R \quad \varphi_R]_{-k}(\omega^2[\rho_0]-k^2[K_0])k^2\begin{bmatrix}\phi_R\\\varphi_R\end{bmatrix}_k+[A_R \quad a_R]^m_{-k}(\omega^2[\rho_0]-k^2[\mu_0])(k^2\delta^{mn}-k^mk^n)\begin{bmatrix}A_R\\a_R\end{bmatrix}^n_k\right\}. \tag{31}$$

Though experimentally one might be inclined to express fluctuations in terms of the laboratory parameters of Sec. II, a great simplification is obtained in understanding both the free Biot theory and its renormalization group flow by choosing a different basis, which of course represents all the same information. The decomposition used here follows the observation that general, symmetric 2×2 matrices may be expanded as $[\rho']=\rho'_\alpha\sigma^\alpha$, $[\lambda']=\lambda'_\alpha\sigma^\alpha$, $[\mu']=\mu'_\alpha\sigma^\alpha$, $\alpha\in(0,\ldots,2)$ summed, where

$$\sigma^0 \equiv \begin{bmatrix} 1 & \\ & 1 \end{bmatrix}, \quad \sigma^1 \equiv \begin{bmatrix} & 1 \\ 1 & \end{bmatrix}, \quad \sigma^2 \equiv \begin{bmatrix} 1 & \\ & -1 \end{bmatrix}. \tag{32}$$

In the σ-matrix basis, determinants have the simple expression $|\rho'| = \rho'^2_0 - \rho'^2_1 - \rho'^2_2$, showing that the coefficients ρ'_α (etc.) are coordinates in a three-dimensional space, on which the determinant defines an SO(2,1) norm.

The remaining terms in Eq. (24), after subtraction of Eq. (31), may be written as

$$L^{\text{pert}} \equiv \frac{1}{2}\int \frac{d^d k\, d^d k'}{(2\pi)^{2d}} [\rho'_\alpha \quad \lambda'_\alpha \quad \mu'_\alpha]_{k-k'} \begin{bmatrix} \omega^2 R^\alpha_R \\ -L^\alpha_R \\ -M^\alpha_R \end{bmatrix}_{k,k'}, \tag{33}$$

with the definitions of moments in the potentials:

$$R^\alpha_{Rk,k'} \equiv \left\{ [\phi_R \quad \varphi_R]_{-k} \sigma^\alpha \begin{bmatrix} \phi_R \\ \varphi_R \end{bmatrix}_{k'} (k\cdot k') + 2[\phi_R \quad \varphi_R]_{-k} \sigma^\alpha \begin{bmatrix} A_R \\ a_R \end{bmatrix}^n_{k'} \epsilon^{jln} k^j k'^l + [A_R \quad a_R]^m_{-k} \sigma^\alpha \begin{bmatrix} A_R \\ a_R \end{bmatrix}^n_{k'} (k\cdot k' \delta^{mn} - k'^m k^n) \right\}, \tag{34}$$

$$L^\alpha_{Rk,k'} \equiv \left\{ [\phi_R \quad \varphi_R]_{-k} \sigma^\alpha \begin{bmatrix} \phi_R \\ \varphi_R \end{bmatrix}_{k'} (k^2 k'^2) \right\}, \tag{35}$$

$$M^\alpha_{Rk,k'} \equiv \left\{ 2[\phi_R \quad \varphi_R]_{-k} \sigma^\alpha \begin{bmatrix} \phi_R \\ \varphi_R \end{bmatrix}_{k'} (k\cdot k')^2 + 4[\phi_R \quad \varphi_R]_{-k} \sigma^\alpha \begin{bmatrix} A_R \\ a_R \end{bmatrix}^n_{k'} (k\cdot k') \epsilon^{jln} k^j k'^l \right.$$
$$\left. + [A_R \quad a_R]^m_{-k} \sigma^\alpha \begin{bmatrix} A_R \\ a_R \end{bmatrix}^n_{k'} [k\cdot k' (k\cdot k' \delta^{mn} - k'^m k^n) - \epsilon^{ikm} k^i k'^k \epsilon^{jln} k^j k'^l] \right\}. \tag{36}$$

The spectrum of background fluctuations is defined by the weight function in Eq. (28). The simplest choice, and one representing the generic leading-order terms in a replica expansion,[13] is a Gaussian distribution with δ-function position correlations, obtained when

$$L^{\text{weight}} \equiv \frac{1}{2}\int \frac{d^d k}{(2\pi)^d} [\rho'_\alpha \quad \Lambda'_\alpha \quad \mu'_\alpha]_{-k} [D^{\alpha\beta}] \begin{bmatrix} \rho'_\beta \\ \Lambda'_\beta \\ \mu'_\beta \end{bmatrix}_k. \tag{37}$$

The kernel $[D^{\alpha\beta}]$ in Eq. (37) determines the autocorrelation matrix of the fluctuation coordinates, which may be expressed as the pure statistical average

$$\overline{\begin{bmatrix} \rho'_\beta \\ \lambda'_\beta \\ \mu'_\beta \end{bmatrix}_{x'} [\rho'_\alpha \quad \lambda'_\alpha \quad \mu'_\alpha]_x} = \delta^d(x'-x) G_{\beta\alpha} = \delta^d\left(\frac{x'-x}{l_0}\right) \frac{G_{\beta\alpha}}{l_0^d}, \tag{38}$$

in which $G_{\beta\alpha} D^{\alpha\gamma} \equiv \delta^\gamma_\beta$.

In the second expression on the right-hand side of Eq. (38), the nondimensionalized δ-function becomes the Kronecker δ on patches at the natural scale, so the combination $G_{\beta\alpha}/l_0^d$ may be assigned a physical magnitude from the mean-square parameter fluctuations, in the approximation of spatially uncorrelated heterogeneity.

Completing the square in Eq. (29) by shifting the fields ρ'_α, λ'_α, μ'_α, and cancelling the (now constant) Gaussian integral against $\mathcal{Z}$, gives the standard[2,13] replica representation of the averaged Green's function in the presence of quenched white-noise randomness:

$$\overline{\left\langle \begin{bmatrix} u \\ w \end{bmatrix}^i_{-k'} [u \quad w]^j_k \right\rangle} = \lim_{n\to 0} \int \mathcal{D}\phi_R \mathcal{D}\varphi_R \mathcal{D}A_R \mathcal{D}a_R e^{-L^{\text{free}} - L^{\text{int}}} \begin{bmatrix} u \\ w \end{bmatrix}^i_{(1),-k'} [u \quad w]^j_{(1),k}, \tag{39}$$

in which the interaction Lagrangian

$$L^{\text{int}} \equiv -\frac{1}{8}\int \frac{d^d k_1 d^d k_2 d^d k_3}{(2\pi)^{3d}} [\omega^2 R_R^\alpha \quad -L_R^\alpha \quad -M_R^\alpha]_{k_1,k_2} [G_{\alpha\beta}] \begin{bmatrix} \omega^2 R_R^\beta \\ -L_R^\beta \\ -M_R^\beta \end{bmatrix}_{k_3,k_4} \tag{40}$$

is now quartic in the fields, and $k_4 \equiv k_1 - k_2 + k_3$. The same construction, with somewhat more work but no change in form, can readily be generalized to model spatially correlated disorder. To do so, $[G_{\alpha\beta}]$ is given explicit wave number dependence, as in Ref. 28 for spatially power-law correlated fluctuations.

The negative-semidefinite interaction (40) renders the functional integral (39) divergent, if the fields are integrated along real hypercontours. Equation (39) is therefore defined[13] by introducing single-component fields $\phi \equiv \sqrt{-i}\phi_R$, $\varphi \equiv \sqrt{-i}\varphi_R$, $A \equiv \sqrt{-i}A_R$, $a \equiv \sqrt{-i}a_R$, and rotating ϕ, φ, A, and a to be integrated along real hypercontours. The free action is expressed in terms of rotated fields as

$$L^{\text{free}} = \frac{i}{2}\int \frac{d^d k}{(2\pi)^d} \left\{ [\phi \quad \varphi]_{-k} (\omega^2[\rho_0] - k^2[K_0]) k^2 \begin{bmatrix} \phi \\ \varphi \end{bmatrix}_k + [A \quad a]^m_{-k} (\omega^2[\rho_0] - k^2[\mu_0])(k^2\delta^{mn} - k^m k^n) \begin{bmatrix} A \\ a \end{bmatrix}^n_k \right\}, \tag{41}$$

giving free propagators for compressional and shear potentials of

$$\left\langle \begin{bmatrix} \phi \\ \varphi \end{bmatrix}_{k'} [\phi \quad \varphi]_{-k} \right\rangle^{\text{free}} = \frac{-i(2\pi)^d \delta^d(k'-k)}{k^2} (\omega^2[\rho_0] - k^2[K_0])^{-1} \tag{42}$$

and

$$\left\langle \begin{bmatrix} A \\ a \end{bmatrix}^m_{k'} [A \quad a]^n_{-k} \right\rangle^{\text{free}} = \frac{-i(2\pi)^d \delta^d(k'-k)}{k^2} (\omega^2[\rho_0] - k^2[\mu_0])^{-1} \frac{(k^2\delta^{mn} - k^m k^n)}{k^2}. \tag{43}$$

The formally positive-semidefinite interaction term

$$L^{\text{int}} = \frac{1}{8}\int \frac{d^d k_1 d^d k_2 d^d k_3}{(2\pi)^{3d}} [\omega^2 R^\alpha \quad -L^\alpha \quad -M^\alpha]_{k_1,k_2} [G_{\alpha\beta}] \begin{bmatrix} \omega^2 R^\beta \\ -L^\beta \\ -M^\beta \end{bmatrix}_{k_3,k_4}, \tag{44}$$

now gives a convergent functional integral, with R^α, M^α, and L^α, defined as in Eqs. (34)–(36), but using $\phi_R \to \phi$, $\varphi_R \to \varphi$, $A_R \to A$, and $a_R \to a$.

III. THE RENORMALIZATION GROUP MAP

Equation (39) defines the ensemble-averaged Green's function in terms of bare displacement fields u, w, the bare interaction (44), and an implicit wave number cutoff $\Lambda_0 \equiv 2\pi/l_0$, representing the fact that no fields are defined with Fourier components higher than Λ_0 (spatial resolution finer than l_0). The Green's function for wavelengths much longer than l_0 is not *a priori* well approximated by a low-order perturbative expansion, because of the large domain of wave number integration in scattering loop integrals. This domain is reduced, and in the process, high orders of perturbation theory are summed, by iterating a Wilsonian renormalization group map.[1]

The RG transformation begins by nondimensionalizing wave numbers in each iteration at the largest scale that appears in loop integrals, a running label denoted Λ. Perturbative corrections from wave numbers between $\Lambda - \delta\Lambda$ and Λ are then incorporated in corrected coefficients ("integrated out"), which are finally nondimensionalized with respect to $\Lambda - \delta\Lambda$ to begin the next iteration. The iterated map generates a flow of nondimensionalized coefficients, which is followed until either perturbation theory breaks down, or Λ lies just above the experimental wave numbers of interest. The effective fields and coefficients are then redimensionalized to match the bare fields of Eq. (39). The resulting effective perturbation theory gives, at low orders, realistic estimates of the strength of scattering corrections, because the volume of wave number integration is small, and all relevant information about the natural scale is contained in the coupling strengths themselves.

The RG map thus intertwines classical and perturbative scaling corrections. The leading order of relevance of bare couplings is estimated from their classical scaling dimensions,[29] which are catalogued in this section. The method will be demonstrated using a truncation of the Biot theory to a single compressional potential, which carries the dimensional information of the full compressional sector in a reduced notation. Considering only compression leads to a naive implementation of the so-called "poroacoustic" limit, usually associated with vanishing of the shear modulus.[17] While not valid by itself, this limit illustrates many features

of the more general case, in a tractable form. Transverse excitations will be considered in Sec. VII, as inducing modifications to the scaling derived here.

A. Classical dimensions: A scale model

The truncation of free action (41) to the ϕ-compressional sector may be written

$$L^{\phi}=\frac{i}{2}\int \frac{d^dk}{(2\pi)^d}\phi(\omega^2\rho_0-k^2K_0)k^2\phi. \tag{45}$$

The autocorrelation matrix $[G]$ may be schematically decomposed as

$$[G]\equiv\begin{bmatrix} G^{\rho\rho} & G^{\rho\lambda} & G^{\rho\mu} \\ G^{\lambda\rho} & G^{\lambda\lambda} & G^{\lambda\mu} \\ G^{\mu\rho} & G^{\mu\lambda} & G^{\mu\mu} \end{bmatrix}. \tag{46}$$

The wave number content of scattering terms in A, a is the same as that of ϕ, φ at nonvanishing shear modulus, so the scaling dimensions deduced here for ϕ will carry over to φ and shear in the general case. It will further be shown below that when shear modulus vanishes, interactions involving A, a are always less relevant than those for ϕ, φ. Therefore it is sufficient to consider only the ρ-λ sector of Eq. (46) to deduce all relevant scaling dimensions.

Without loss of generality, $G^{\lambda\rho}=G^{\rho\lambda}$, so from Eq. (44) it is sufficient to consider only the three classes of interaction

$$L^{\rho\rho}=\frac{1}{8}\int \frac{d^dk_1d^dk_2d^dk_3}{(2\pi)^{3d}}(\phi_{-k_1}\cdot\phi_{k_2})(k_1\cdot k_2)\omega^4G_0^{\rho\rho}(k_3\cdot k_4)\times(\phi_{-k_3}\cdot\phi_{k_4}), \tag{47}$$

$$L^{\rho\lambda}=\frac{1}{4}\int \frac{d^dk_1d^dk_2d^dk_3}{(2\pi)^{3d}}(\phi_{-k_1}\cdot\phi_{k_2})\times(k_1\cdot k_2)\omega^2G_0^{\rho\lambda}k_3^2k_4^2(\phi_{-k_3}\cdot\phi_{k_4}), \tag{48}$$

and

$$L^{\lambda\lambda}=\frac{1}{8}\int \frac{d^dk_1d^dk_2d^dk_3}{(2\pi)^{3d}}(\phi_{-k_1}\cdot\phi_{k_2})\times k_1^2k_2^2G_0^{\lambda\lambda}k_3^2k_4^2(\phi_{-k_3}\cdot\phi_{k_4}), \tag{49}$$

for a single σ-component, where the dots between fields denote replica contraction (since Biot two-vectors are no longer available to carry that information).

Starting from Λ_0, the initial values of nondimensionalized fields and couplings are introduced as $\phi\Lambda_0^{d/2+2}\equiv\tilde{\phi}_0/\zeta_0$, $\omega^2\rho_0/\Lambda_0^2=\alpha_0$. In order to reexpress the theory as one of the same form in which the maximal wave number is reduced from $\Lambda_0\to\Lambda_0-\delta\Lambda\equiv\Lambda$, the four stages of an infinitesimal RG map are carried out on the action. The first iteration of this map, acting on the free action defined with Λ_0, takes the form (omitting unneeded wave number indices on fields)

$$\begin{aligned} L^{\phi}&=\frac{i}{2}\int \frac{d^dk}{(2\pi\Lambda_0)^d}\left[\frac{\tilde{\phi}_0}{\zeta_0}\right]^2\frac{k^2}{\Lambda_0^2}\left[\alpha_0-\frac{k^2}{\Lambda_0^2}K_0\right] \\ &=\frac{i}{2}\int \frac{d^dk}{(2\pi)^d}\phi^2k^2[\omega^2\rho_0-k^2K_0] \\ &\to\frac{i}{2}\int \frac{d^dk}{(2\pi)^d}\phi^2k^2[\omega^2(\rho_0+\delta\rho)-k^2(K_0+\delta K)] \\ &=\frac{i}{2}\int \frac{d^dk}{(2\pi\Lambda)^d}\left[\frac{\tilde{\phi}_0}{\zeta_0}\left(\frac{\Lambda}{\Lambda_0}\right)^{d/2+2}\sqrt{1+\delta K/K_0}\right]^2\frac{k^2}{\Lambda^2}\left[\left(\frac{\Lambda_0}{\Lambda}\right)^2\left(\frac{\alpha_0+\delta\alpha}{1+\delta K/K_0}\right)-\frac{k^2}{\Lambda^2}K_0\right]. \end{aligned} \tag{50}$$

The first line of Eq. (50) identifies the nondimensionalized coefficients α_0, ζ_0, and is simply reexpressed in terms of physical fields in the second line. Transformation to the third line is by integration out of high-wave-number field components, which leads to the perturbative corrections $\delta\rho$ and δK (computed explicitly below). In order to leave the wave-number-dominated free propagator in canonical form, the modulus is coerced to remain at K_0, and the shift absorbed in field renormalization, after which the integral is renondimensionalized to arrive at the fourth line.

Equation (50) defines a map of coefficients that depends only on the ratio $(\Lambda+\delta\Lambda)/\Lambda$ and the initial values of the parameters appearing in the free and interaction Lagrangians. This map may be iterated to reduce the wave number cutoff by any multiple of $\delta\Lambda$. As $\delta\Lambda\to0$, infinitely many iterations are required to shift the cutoff by any finite amount, so a continuous reduction in cutoff may be associated with a continuous flow in the nondimensionalized parameter space. It is thus possible to define one-parameter families ζ, α, with $\zeta(\Lambda_0)\equiv\zeta_0$, $\alpha(\Lambda_0)\equiv\alpha_0$, and to resolve the transformation (50) to the differential iteration rules

$$\zeta\to\left(1+\frac{\delta\Lambda}{\Lambda}\right)^{d/2+2}\frac{\zeta}{\sqrt{(1+\delta K/K)}}, \tag{51}$$

$$\alpha\to\left(1+\frac{\delta\Lambda}{\Lambda}\right)^{2}\frac{\alpha+\delta\alpha}{1+\delta K/K}. \tag{52}$$

Application of the same sequence of operations to Eqs. (47)–(49) gives initial values of the nondimensionalized coupling parameters: $\Gamma^{\rho\rho}(\Lambda_0)\equiv(1/8)\omega^4 G_0^{\rho\rho}\Lambda_0^{d-4}$, $\Gamma^{\rho\lambda}(\Lambda_0)\equiv(1/8)\omega^2 G_0^{\rho\lambda}\Lambda_0^{d-2}$, $\Gamma^{\lambda\lambda}(\Lambda_0)\equiv(1/8)\omega^2 G_0^{\lambda\lambda}\Lambda_0^{d}$, and the corresponding flow equations

$$\Gamma^{\rho\rho}\to\left(1+\frac{\delta\Lambda}{\Lambda}\right)^{4-d}\frac{\Gamma^{\rho\rho}+\delta\Gamma^{\rho\rho}}{(1+\delta K/K)^2}, \tag{53}$$

$$\Gamma^{\rho\lambda}\to\left(1+\frac{\delta\Lambda}{\Lambda}\right)^{2-d}\frac{\Gamma^{\rho\lambda}+\delta\Gamma^{\rho\lambda}}{(1+\delta K/K)^2}, \tag{54}$$

and

$$\Gamma^{\lambda\lambda}\to\left(1+\frac{\delta\Lambda}{\Lambda}\right)^{-d}\frac{\Gamma^{\lambda\lambda}+\delta\Gamma^{\lambda\lambda}}{(1+\delta K/K)^2}. \tag{55}$$

In $d=3$, $\Gamma^{\rho\lambda}$ and $\Gamma^{\lambda\lambda}$ are classically irrelevant, so any perturbative corrections to the dispersion relation are contributed only in a close neighborhood of the natural scale. If these corrections are assumed to already be taken into account in the initial values of ρ_0 and K_0, the couplings $\Gamma^{\rho\lambda},\Gamma^{\lambda\lambda}$ can simply be ignored in computing the low wave number RG flow. A further great simplification is obtained if $\rho\rho$ corrections to $[K]$ can be ignored. In the scalar case, this holds for RG flow at all wave numbers much larger than the experimental wave number, because the small parameter $(\omega/c\Lambda)\ll 1$ is the ratio of fractional corrections to K relative to those of α. It will be assumed for the matrix-valued flow here, as long as $\Lambda\gg\omega/c_s$ (the slow wave speed). Then, the irrelevance $\Gamma^{\rho\lambda},\Gamma^{\lambda\lambda}\to 0\Rightarrow\delta K\to 0$.

The resulting, greatly simplified RG equations can immediately be mapped to the full compressional sector, with $\alpha\to[\alpha]$, $\Gamma^{\rho\rho}\to\Gamma^{\rho\rho}_{\alpha\beta}$. Correct to leading order in $\delta\Lambda/\Lambda$, which will later be taken to zero,

$$[\alpha]\to\left(1+\frac{\delta\Lambda}{\Lambda}\right)^{2}[\alpha]+[\delta\alpha], \tag{56}$$

$$\Gamma^{\rho\rho}_{\alpha\beta}\to\left(1+\frac{\delta\Lambda}{\Lambda}\right)^{4-d}\Gamma^{\rho\rho}_{\alpha\beta}+\delta\Gamma^{\rho\rho}_{\alpha\beta}. \tag{57}$$

B. Graph expansion of the relevant sector

The perturbative corrections in Eqs. (56) and (57) are computed by splitting $\phi=\phi_0+\phi'$, $\varphi=\varphi_0+\varphi'$, $A=A_0+A'$, and $a=a_0+a'$, where $(\,)_0$ components have only wave numbers less than $\Lambda-\delta\Lambda$, and $(\,)'$ only those between $\Lambda-\delta\Lambda$ and Λ. The interaction exponential is expanded as a power series,

$$e^{-L^{\rm int}}=\sum_{i=0}^{\infty}\frac{(-L^{\rm int})^i}{i!}, \tag{58}$$

and $(\,)'$-Green's functions are evaluated at one-loop order. Since only $\rho\rho$ interactions are relevant, coupling notation will be simplified by taking $G^{\rho\rho}_{\alpha\beta}\to G_{\alpha\beta}$.

At this point, attention will be restricted to the naive interpretation of the ''poroacoustic'' sector,[17] in which transverse excitations are simply ignored. This limit is often assumed (more correctly) in sea floor sediment scattering processes. It will be shown in Sec. VII that, in the limit $\mu\to 0$, corrections from the shear propagator are classically irrelevant, making it look like these may be incorporated consistently in initial conditions like effects from $\Gamma^{\rho\lambda},\Gamma^{\lambda\lambda}$ above. This limit is actually not valid as an extrapolation all the way from the natural scale, though, because while transverse excitations may have irrelevant couplings, they are initially larger than longitudinal ones.

The naive poroacoustic limit is nevertheless a very interesting starting point, because it appears to be the largest sector about which anything general can be said based on scaling dimensions alone. It also can emerge as the appropriate scaling theory in the proper $\mu\to 0$ analysis, at some scale well below the natural scale. These issues will be addressed Sec. VII.

The only terms appearing in connected, one-loop $[\phi^0\ \varphi^0]$ graphs come from the second-order expansion in primes. These terms in $L^{\rm int}$ will be considered in slightly more general form than appears in the bare interaction (44):

$$L^{\rm int}\ni\frac{1}{8}\int\frac{d^dk_1d^dk_2d^dk_3}{(2\pi)^{3d}}\omega^4G_{\alpha\beta}\Bigg\{2\,[\phi\quad\varphi]^0_{-k_1}\sigma^\alpha\begin{bmatrix}\phi\\ \varphi\end{bmatrix}^0_{k_2}\,[\phi\quad\varphi]'_{-k_3}\sigma^\beta\begin{bmatrix}\phi\\ \varphi\end{bmatrix}'_{k_4}$$
$$+4\,[\phi\quad\varphi]^0_{-k_1}\sigma^\alpha\begin{bmatrix}\phi\\ \varphi\end{bmatrix}'_{k_2}\,[\phi\quad\varphi]^0_{-k_3}\sigma^\beta\begin{bmatrix}\phi\\ \varphi\end{bmatrix}'_{k_4}\Bigg\}\{(k_1\cdot k_2)(k_3\cdot k_4)+\xi[(k_1\cdot k_3)(k_2\cdot k_4)+(k_1\cdot k_4)(k_2\cdot k_3)]\}. \tag{59}$$

$\xi=0$ gives the bare vertex, while the most general interactions can in principle generate different values of ξ for each component of $G_{\alpha\beta}$. [Note, however, that because the two terms in Eq. (59) at a single component of $G_{\alpha\beta}$ come from division of a single field arbitrarily by wave number, the value of ξ for both terms must be the same.] Equation (59) is sufficient for analysis of stationary rays of the RG flow, without introducing the full complexity of the most general form.

Figure 1 represents the interactions in Eq. (59) graphically. Replica-index contraction is denoted by continuity of solid lines; this is what makes replica-field RG flow different from the canonical s^4 model.[1] In a model with spatially correlated roughness,[28] the autocorrelation $G_{\alpha\beta}$, indicated by a

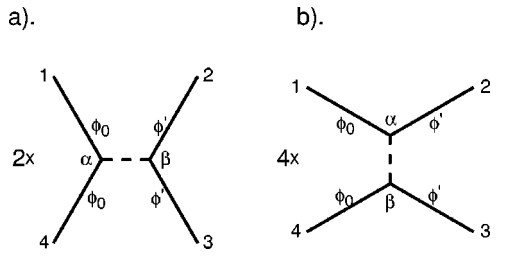

FIG. 1. Vertices associated with the decomposition (59). Solid lines connected through points indicate replica-field contractions; dashed line indicates coupling $G_{\alpha\beta}$.

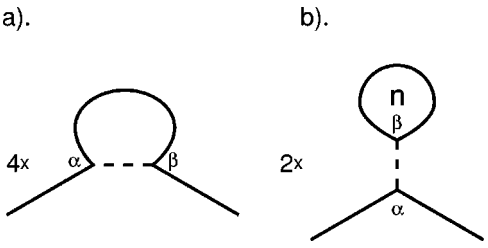

FIG. 2. Two graphs that renormalize density matrix $[\alpha]$ at finite *n*. Direct graph (a) is $\mathcal{O}(n^0)$; bubble graph (b) is $\mathcal{O}(n^1)$, and vanishes at $n\to 0$.

dashed line, would resemble a conventional dynamical propagator in having nontrivial wave number dependence.

IV. PERTURBATIVE RENORMALIZATION OF THE NAIVE POROACOUSTIC SECTOR

The vertices in Fig. 1 define a graph expansion of the compressional propagator and interactions. Straight lines denote the full Biot-vector field $[\phi^0 \;\; \varphi^0]$. The two graphs that correct the propagator at general *n* are shown in Fig. 2. The second graph is $\mathcal{O}(n^1)$, because *n* replica fields are free to propagate around the bubble. The first graph is $\mathcal{O}(n^0)$ because of replica contraction with the external index. Thus only the direct graph, incorporating the vertex in Fig. 1(b), contributes as $n\to 0$.

Because the RG is intended to identify the general features of the most dominant scattering corrections, the propagator at wave numbers much larger than physical ω/c values will be replaced by the K_0 terms only, and inner products of loop with external wave numbers will be kept only to leading order in the (large) loop wave numbers. Higher-order terms in the ratio of external to internal wave numbers generate higher-derivative corrections to the dispersion relation, which are classically irrelevant compared to the terms that are kept. This approximation is necessary because the RG cannot make all the complexity of higher order graphs go away; it simply enables one to organize it and extract the leading dependence.

If RG flow is assumed to keep the components of *G* homogeneous in ξ, the propagator correction may be evaluated without further approximation. Using $d=3$ to simplify integrals like $\int_{\Lambda-\delta\Lambda}^{\Lambda} d^d k/(2\pi)^d = \Lambda^{d-1}\delta\Lambda/2\pi^2$, the graph in Fig. 2(a) gives

$$[\delta\alpha] = \frac{8}{2\pi^2}\Gamma_{\alpha\beta}\sigma^\alpha [K_0]^{-1}\sigma^\beta\left(\frac{1}{3}+\frac{4}{3}\xi\right)\frac{\delta\Lambda}{\Lambda}. \tag{60}$$

The three types of graph that correct the interaction vertex at general *n* are shown in Fig. 3. These become very complicated if the most general vertex is input, so they will be computed here from the simpler form of Eq. (59). By convention, the wave numbers of fields connected by replica contraction will be paired as (k_1,k_2) and (k_3,k_4). Once again, the bubble graph vanishes as $n\to 0$, which is the replica manifestation that roughness renormalizes the acoustic interactions, but sound does not renormalize the roughness distribution, indicated by the dashed line.

Evaluating the graphs in Fig. 3 as iterations in $\Gamma_{\alpha\beta}$ and ξ is easiest if one introduces explicit indices to track σ matrices:

$$\sigma^\alpha \equiv [\sigma^\alpha_{ab}]_{a,b=1,2}. \tag{61}$$

Denoting by $\delta\Gamma_{\alpha\beta}$ the change in coefficient of the replica-respecting wave number dot products, the evaluation at $n\to 0$ and $d=3$ is

$$\delta\Gamma_{\alpha\beta}\sigma^\alpha_{ab}\sigma^\beta_{cd} = \frac{16}{2\pi^2}\Gamma_{\alpha\beta}\Gamma_{\gamma\delta}\Bigg\{(\sigma^\alpha[K_0]^{-1}\sigma^\gamma)_{ab}(\sigma^\delta[K_0]^{-1}\sigma^\beta)_{cd}\left(\frac{1}{15}+\frac{2}{15}\xi+\frac{1}{15}\xi^2\right)$$
$$+[\sigma^\alpha_{ab}(\sigma^\gamma[K_0]^{-1}\sigma^\beta[K_0]^{-1}\sigma^\delta)_{cd}+(\sigma^\alpha[K_0]^{-1}\sigma^\gamma[K_0]^{-1}\sigma^\beta)_{ab}\sigma^\delta_{cd}]\left(\frac{1}{6}+\frac{11}{15}\xi+\frac{2}{5}\xi^2\right)\Bigg\}\frac{\delta\Lambda}{\Lambda}. \tag{62}$$

By an abuse of notation, the evolution of the remaining coefficient, of replica-violating wave number products, is

$$\delta(\xi\Gamma_{\alpha\beta})\sigma^\alpha_{ab}\sigma^\beta_{cd} = \frac{16}{2\pi^2}\Gamma_{\alpha\beta}\Gamma_{\gamma\delta}\Bigg\{(\sigma^\alpha[K_0]^{-1}\sigma^\gamma)_{ab}(\sigma^\delta[K_0]^{-1}\sigma^\beta)_{cd}\left(\frac{1}{15}+\frac{7}{15}\xi+\frac{9}{10}\xi^2\right)+[\sigma^\alpha_{ab}(\sigma^\gamma[K_0]^{-1}\sigma^\beta[K_0]^{-1}\sigma^\delta)_{cd}$$
$$+(\sigma^\alpha[K_0]^{-1}\sigma^\gamma[K_0]^{-1}\sigma^\beta)_{ab}\sigma^\delta_{cd}]\left(\frac{1}{15}\xi+\frac{1}{15}\xi^2\right)\Bigg\}\frac{\delta\Lambda}{\Lambda}. \tag{63}$$

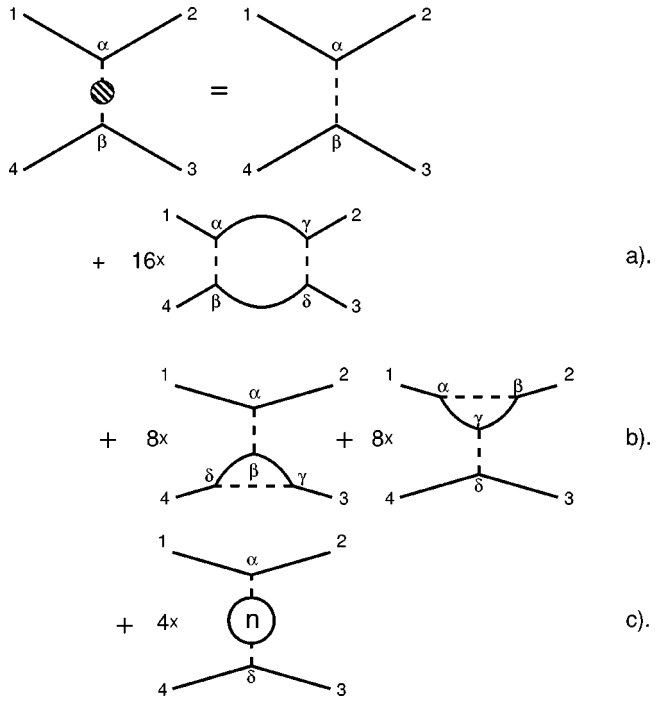

FIG. 3. Three graphs that renormalize $G_{\alpha\beta}$ at finite n. Box (a) and penguin (b) are $\mathcal{O}(n^0)$; bubble (c) is $\mathcal{O}(n^1)$, and vanishes at $n\to 0$.

V. STATIONARY RAYS OF THE EFFECTIVE INTERACTION

For general matrix products of σ^α and $[K_0]^{-1}$, Eq. (63) does not resolve to a separable evolution of ξ and $\Gamma_{\alpha\beta}$, because replica-respecting and replica-violating dot products are mixed with different interaction matrices in different ways. Further, at any fixed value of ξ, the form of the interaction vertices is not generally preserved, so the full RG flow is very complicated to analyze.

One exception to this complexity, which corresponds to the fixed points in stable systems, occurs when the starting interaction is a dyadic of certain matrices:

$$\Gamma_{\alpha\beta}\sigma^\alpha_{ab}\sigma^\beta_{cd}=\Gamma\sigma^*_{ab}\sigma^*_{cd}. \tag{64}$$

The condition that the box diagram [Fig. 3(a), which automatically produces dyadic corrections] create shifts proportional to Eq. (64) implies that, for a scalar κ,

$$\sigma^*[K_0]^{-1}\sigma^*=\kappa\sigma^*, \tag{65}$$

which may be checked to imply in turn that σ^* is degenerate, or lightlike in the SO(2,1) description.[30] Condition (65) also ensures that the penguin diagrams [Fig. 3(b)] are proportional to the same dyadic, because σ^* acts on $[K_0]^{-1}$ by projection.

The conditions (64) and (65) define *stationary rays* of the poroacoustic RG flow. Along these rays at general ξ, Eq. (62) reduces to

$$\delta\Gamma=\frac{16}{2\pi^2}\Gamma^2\kappa^2\left(\frac{2}{5}+\frac{8}{5}\xi+\frac{13}{15}\xi^2\right)\frac{\delta\Lambda}{\Lambda}. \tag{66}$$

Further, ξ and Γ separate, so Eq. (63), with Eq. (62), implies that

$$\delta\xi=\frac{16}{2\pi^2}\Gamma\kappa^2\left(\frac{1}{15}+\frac{1}{5}\xi-\frac{17}{30}\xi^2-\frac{13}{15}\xi^3\right)\frac{\delta\Lambda}{\Lambda}. \tag{67}$$

Evolution equation (67) for positive ξ has a unique, stable fixed point ($\delta\xi=0$) at $\xi=\xi^*\approx 0.86$, so the asymptotic perturbative corrections may be evaluated in terms of Γ, Λ, and ξ^*.

With these simplifications, it becomes convenient to combine classical and perturbative RG corrections into one-parameter flow equations (the so-called ''beta functions'') for each dimensionless coefficient. The scale-change increment $-\delta\Lambda$ is reduced to a differential of the logarithm of scale, $\delta\Lambda/\Lambda\to -d\log(\Lambda)$, and Eqs. (57) and (66) are combined to read

$$-\frac{d\Gamma}{d\log(\Lambda)}=(4-d)\Gamma+\frac{8}{\pi^2}\Gamma^2\kappa^2\left(\frac{2}{5}+\frac{8}{5}\xi^*+\frac{13}{15}\xi^{*2}\right), \tag{68}$$

where the combination $(2/5+8\xi^*/5+13\xi^{*2}/15)\approx 2.42$.

Flow equation (68) has solution

$$\Gamma=\frac{\Gamma_0\left(\frac{\Lambda_0}{\Lambda}\right)^{4-d}}{1-\frac{8}{\pi^2}\kappa^2\Gamma_0\left(\frac{2}{5}+\frac{8}{5}\xi^*+\frac{13}{15}\xi^{*2}\right)\left[\frac{(\Lambda_0/\Lambda)^{4-d}-1}{4-d}\right]}, \tag{69}$$

where d (here 3) is left explicit for contact with the conventional ϵ expansion.[1,13]

The notational reduction and dyadic form (64), in terms of the dimensional coupling, are $G^{\rho\rho}_{\alpha\beta}\sigma^\alpha_{ab}\sigma^\beta_{cd}\to G\sigma^*_{ab}\sigma^*_{cd}$. Redimensionalizing Γ, the effective coupling appearing in a renormalized interaction (44) is

$$G_0\to G^{\rm eff}(\Lambda)=\frac{G_0}{1-\frac{8}{\pi^2}\kappa^2\Gamma_0\left(\frac{2}{5}+\frac{8}{5}\xi^*+\frac{13}{15}\xi^{*2}\right)\left[\frac{(\Lambda_0/\Lambda)^{4-d}-1}{4-d}\right]}. \tag{70}$$

$\kappa^2\Gamma_0=\kappa^2\omega^4G_0\Lambda_0^{d-4}/8$ is the dimensionless small parameter in the bare theory that controls where $G^{\rm eff}$ becomes large. For dimensions near four, the term in square brackets in the denominator reduces to a logarithm, so there is a potentially large separation of scales between the natural scale and the wavelength of strong coupling. In $d=3$, however,

this separation is of order $1/\kappa^2\Gamma_0$, which may be only a few orders of magnitude even for small bare coupling. In $d=3$, it is convenient to define a critical scale as

$$\Lambda_C=\Lambda_0\frac{\frac{8}{\pi^2}\kappa^2\Gamma_0\left(\frac{2}{5}+\frac{8}{5}\xi^*+\frac{13}{15}\xi^{*2}\right)}{1+\frac{8}{\pi^2}\kappa^2\Gamma_0\left(\frac{2}{5}+\frac{8}{5}\xi^*+\frac{13}{15}\xi^{*2}\right)}, \tag{71}$$

and reexpress Eq. (70) as

$$G^{\rm eff}(\Lambda)=G_0\frac{1-\Lambda_C/\Lambda_0}{1-\Lambda_C/\Lambda}. \tag{72}$$

Equation (69) may be substituted into the corresponding flow equations (56) and (60) for the density matrix,

$$-\frac{d[\alpha]}{d\log(\Lambda)}=2[\alpha]+\frac{4}{\pi^2}\Gamma\kappa\sigma^*\left(\frac{1}{3}+\frac{4}{3}\xi^*\right), \tag{73}$$

and solved exactly in $d=3$ to give

$$\begin{aligned}[\rho_0]\rightarrow[\rho^{\rm eff}](\Lambda)=&[\rho_0]+\frac{\kappa}{2\pi^2}\sigma^*(\omega^2G_0\Lambda_0^{d-2})\\&\times\left(\frac{1}{3}+\frac{4}{3}\xi^*\right)\left(1-\frac{\Lambda_C}{\Lambda_0}\right)\\&\times\left[1-\frac{\Lambda}{\Lambda_0}+\frac{\Lambda_C}{\Lambda_0}\log\left(\frac{\Lambda_0-\Lambda_C}{\Lambda-\Lambda_C}\right)\right],\end{aligned} \tag{74}$$

where $(1/3+4\xi^*/3)\approx 1.5$.

Equation (74) shows that strong coupling leads to strong correction of the dispersion relation, in which the density diverges by a term proportional to σ^*. The relation of σ^* to the eigenvalue κ of Eq. (65) will show how this isolates the slow wave, while leaving the fast wave finitely perturbed.

VI. EFFECTIVE DISPERSION AND THE SLOW WAVE

A. Biot solutions and the light cone

The SO(2,1) structure of 2×2 real, symmetric matrices with determinant norm proves very useful in visualizing Biot solutions, both in the free theory and with renormalization corrections. The fundamental observation is that matrices with a zero eigenvalue form ''light cones''[30] in the $(\sigma^0,\sigma^1,\sigma^2)$ basis, which separate the space into three connected components.

The number of Biot solutions, in terms of modulus and density determinants, can immediately be understood. Conventional values of Biot parameters for fluids in granular solids[18,31] give $|K_0|>0$, $|\rho_0|>0$. The matrix $\omega^2[\rho_0]$ thus lies in the upper light cone (axis $+\sigma^0$), and $-[K_0]$ lies in the lower light cone. Biot compressional waves are eigenvectors of $\omega^2[\rho_0]-k^2[K_0]$ with zero eigenvalue. Since this kernel starts at $k^2=0$ in the upper light cone, and adds an arbitrarily large negative timelike component (proportional to $-[K_0]$), there are exactly two solutions, where the kernel exits the upper light cone and enters the lower one. Similarly, because the shear modulus matrix $[\mu_0]$ is lightlike, the shear kernel has exactly one propagating solution. These dispersion relations are diagrammed in Fig. 4.

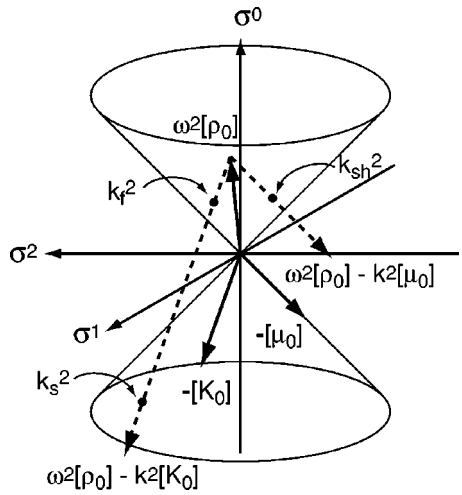

FIG. 4. SO(2,1) structure of the compressional and shear determinants. Basis vectors (axes) are the matrices of Eq. (32). Cones are the set of all zero-determinant matrices. Solid arrows are the three matrix components of any Biot wave equation: $\omega^2[\rho]$, $-[K_0]$, and $-[\mu_0]$, k_f and k_s are respectively fast and slow compressional wave numbers, and k_{sh} is shear wave number. Dots represent solutions to the wave equation, where wave kernels have zero-eigenvalue eigenvectors; there are always two for the compressional kernel, because of how the cones divide the space. Degeneracy of the shear modulus matrix precludes entry into the lower light cone; hence, there is only one shear solution.

B. Dominant stationary ray and the slow wave

The stationary rays solving Eq. (65) can immediately be characterized by decomposing $[K_0]$ into lightlike components. General

$$[K_0]\equiv K_+(v_+v_+^{\rm T})+K_-(v_-v_-^{\rm T}), \tag{75}$$

where v_+ and v_- are eigenvectors with eigenvalues K_+ and K_-, respectively, superscript T denotes transpose, and for positive determinant, $K_+\geqslant K_->0$. The inverse matrix is then

$$[K_0]^{-1}\equiv\frac{1}{K_+}(v_+v_+^{\rm T})+\frac{1}{K_-}(v_-v_-^{\rm T}), \tag{76}$$

and the completeness relation may be written

$$(v_+v_+^{\rm T})+(v_-v_-^{\rm T})=1\equiv\sigma^0, \tag{77}$$

because dyadic matrices are degenerate (lightlike). $[K_0]$ thus defines a plane, with (longitudinal) spacelike axis

$$\sigma^L\equiv(v_+v_+^{\rm T})-(v_-v_-^{\rm T}). \tag{78}$$

If a third, spacelike unit matrix σ^T (transverse) is chosen orthogonal to σ^0 and σ^L, $(\sigma^0,\sigma^L,\sigma^T)$ replace $(\sigma^0,\sigma^1,\sigma^2)$ as

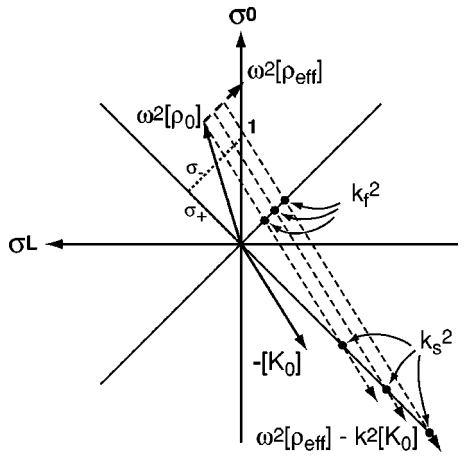

FIG. 5. Renormalization of a density matrix starting in the plane of $[K_0]$, for the case $K_+/K_- > \rho_+/\rho_-$. Solid diagonal lines are again the set of all zero-determinant matrices, and dotted lines show null basis elements $\sigma_\pm$ of $[K_0]$ (and also of $[\rho_0]$ for this case). Heavy dashed line indicates correction by σ_- to $[\rho_0]$ from renormalization. Light dashed lines show compressional kernel matrices as functions of k^2, as in Fig. 4. Dots are again zero determinant solutions k_f^2 (which does not change) and k_s^2 (which diverges), for three successive values of $[\rho_{\text{eff}}]$.

a basis. For uniformity of notation, the outer products appearing in Eq. (77) will be given names $\sigma_\pm \equiv (\sigma^0 \pm \sigma^L)/2$, with $|\sigma_\pm| = 0$.

General lightlike σ^* may now be expressed simply as

$$\sigma^* = \frac{1}{2}(\sigma^0 + \cos(\theta)\sigma^L + \sin(\theta)\sigma^T), \tag{79}$$

and plugging into Eq. (65) gives

$$\kappa = \left(\frac{1-\cos(\theta)}{2K_-} + \frac{1+\cos(\theta)}{2K_+}\right). \tag{80}$$

Not surprisingly, the stationary ray of largest eigenvalue corresponds to $\theta = \pi$, $\sigma^* = \sigma_-$, and $\kappa = 1/K_-$.

The simplest renormalization corrections to visualize involve this largest eigenray and $[\rho_0]$ in the plane of $[K_0]$: that is, $[\rho_0] = \rho_+\sigma_+ + \rho_-\sigma_-$. The ''natural'' case $K_+/K_- > \rho_+/\rho_- \Rightarrow c_s^2 = K_-/\rho_-$ is diagrammed in Fig. 5. Because $[\rho_0]$ lies to the right of $[K_0]$, addition of σ^* causes $[\rho^{\text{eff}}]$ to migrate *parallel* to the light cone pierced at k_f^2, resulting in *no change* in c_f. Migration is orthogonal to, and away from, the light cone pierced at k_s^2, however, driving the slow wave number to infinity and c_s to zero. This only happens asymptotically, though; at no finite integration range does the density become lightlike, or the number of Biot solutions change. Equation (74) diagonalizes simply in this case, and the slow wave speed is given relative to its initial value by

$$\frac{c_s^2(\Lambda_0)}{c_s^2(\Lambda)} = 1 + 4\pi \frac{k_s^2(\Lambda_0)}{\Lambda_0^2}\left(\frac{G_0/l_0^d}{\rho_-^2}\right)\left(\frac{1}{3} + \frac{4}{3}\xi^*\right)\left(1 - \frac{\Lambda_C}{\Lambda_0}\right) \times \left[1 - \frac{\Lambda}{\Lambda_0} + \frac{\Lambda_C}{\Lambda_0}\log\left(\frac{\Lambda_0 - \Lambda_C}{\Lambda - \Lambda_C}\right)\right], \tag{81}$$

where $k_s^2(\Lambda_0) \equiv \omega^2/c_s^2(\Lambda_0)$. Recalling Eq. (38), the coupling term $G_0/l_0^d\rho_-^2$ is simply the fractional squared fluctuation of the density component that participates in the slow wave, on a fundamental patch at the natural scale.

The complementary case $K_+/K_- < \rho_+/\rho_-$, which can be chosen with suitable initial conditions, has a more complicated description, but is not ''natural'' in the sense of being stable under renormalization. If $[\rho_0]$ lies in the same quadrant as $[K_0]$ and is ''more lightlike,'' k_f^2 occurs where the Biot kernel pierces the upper left light cone, and k_s^2 where it pierces the lower left. In this case, addition of σ_+ initially rapidly increases k_f^2, leaving k_s^2 unchanged. However, at finite RG flow there is a cusp, where both solutions transition to piercing the right-hand light cones, and the description reverts to the natural case, with k_f^2 asymptotically unaltered, and k_s^2 diverging.

Renormalization of general $[\rho_0]$ (not in the $[K_0]$-plane) has the same asymptotics as in Fig. 5. For $[\rho_0]$ given ''unnatural'' initial conditions, the cusp to natural behavior is softened, because it does not pass through the vertex of the light cone. It may also easily be checked, for small out-of-plane component, that the fast wave speed is reduced slightly by renormalization, as expected for a scattering correction to the acoustic index of refraction, while the slow wave speed goes to zero slightly more slowly than in the in-plane case.

In all this discussion, it is important to keep in mind that the singular points of RG flows are significant because they assign a specific number to critical coupling strengths and renormalization scales, and give the signs of corrections on the approach to the critical value. However, they come from a set of flow equations that remain integrable far beyond the point where the perturbation theory leading to them becomes invalid. The divergence of Eq. (72) is linear in $\Lambda - \Lambda_C$, while the same divergence in Eq. (81) is logarithmic. Thus, strong coupling is reached while the renormalization of the slow wave speed is of order unity, and perturbation theory does not reliably indicate the degree or direction of further corrections from further scaling. In other words, one never has reason to expect slow wave speed renormalization by more than order unity in the poroacoustic limit of the perturbative RG.

Fine tuning is required to place the initial conditions of the RG flow exactly on any stationary ray. Therefore, the generic case is expected to be nonstationary, with the largest basin of attraction corresponding to the stationary ray of largest eigenvalue. For large difference between K_+ and K_-, all fast-growing rays lie in a neighborhood of $\theta = \pi$, and asymptotic flow for general initial conditions is expected to be toward these rays. Though a full stability analysis seems intractable analytically, stability analyses of simplified cases (Appendix A) support this conclusion.

VII. SHEAR

A. Problems with the naive poroacoustic limit

Evaluation of the critical scale (71) in the range of validity of perturbation theory gives

$$\frac{\Lambda_C c_s(\Lambda_0)}{\omega} \sim 8\pi \left(\frac{G_0/l_0^d}{\rho_-^2} \right) \left(\frac{\omega}{\Lambda_0 c_s(\Lambda_0)} \right)^3. \tag{82}$$

If we ask, when is strong coupling achieved just above the on-shell wave number, this amounts to assuming the wave speed is weakly renormalized, and setting $\Lambda_C \geqslant k_s(\omega) \approx \omega/c_s(\Lambda_0)$. For this to happen at frequencies where the effective medium is sensibly defined, we must also have $\omega/\Lambda_0 c_s(\Lambda_0) \leqslant 1$, so that

$$1 \leqslant \left(\frac{\Lambda_0 c_s(\Lambda_0)}{\omega} \right)^3 \lesssim 8\pi \left(\frac{G_0/l_0^d}{\rho_-^2} \right). \tag{83}$$

In other words, strong coupling is reached within the homogenization regime only when

$$\left(\frac{G_0/l_0^d}{\rho_-^2} \right) \gtrsim \frac{1}{8\pi} \approx 0.04. \tag{84}$$

(This will be demonstrated in the next section.)

Equation (83) has a simple scaling explanation. The combination $\Gamma(\Lambda)/K_-^2$, at any Λ, is just the size of the four-ϕ term at the Gaussian excursions permitted by K_-. When it is $\geqslant 1$ the coupling term, rather than the free wave equation, controls fluctuations, and the perturbation expansion becomes invalid. The classically scaled form of this ratio is

$$\frac{\Gamma(\Lambda)}{K_-^2} = \frac{(2\pi)^d}{8} \left(\frac{G_0/l_0^d}{\rho_-^2} \right) \left(\frac{\omega}{\Lambda c_s(\Lambda_0)} \right)^4 \left(\frac{\Lambda}{\Lambda_0} \right)^d. \tag{85}$$

Equation (83), up to a factor $8/\pi^2$ in $d=3$, is just the condition that Eq. (85) reach unity at $\Lambda \approx k_s(\omega)$.

The same coupling strength for all-transverse excitations at zero shear modulus, using the scaling (56) for $[\alpha]$, is

$$\frac{\Gamma(\Lambda)}{\alpha_-^2} = \frac{(2\pi)^d}{8} \left(\frac{G_0/l_0^d}{\rho_-^2} \right) \left(\frac{\Lambda}{\Lambda_0} \right)^d. \tag{86}$$

In the real poroacoustic limit, Eq. (86) is larger than Eq. (85) at all Λ between the natural scale and $k_s(\omega)$, and cannot be ignored. There is a way to regulate the perturbation theory controlled by Eq. (86), and in some special cases this can even be extended into the region of nonvanishing shear modulus.

B. Proper poroacoustic scaling

A natural way to analyze the relation between longitudinal and transverse scattering at $\mu \to 0$ follows from the nondimensionalized form of Eq. (41). Using tildes, as before, to indicate nondimensionalized fields, and introducing separate wave function normalizations ζ^ϕ and ζ^A for compression and shear, respectively,

$$L^{\text{free}} = \frac{i}{2} \int \frac{d^d k}{(2\pi\Lambda)^d} \left\{ (\zeta^\phi)^{-2} [\tilde{\phi} \quad \tilde{\varphi}]_{-k} \right.$$
$$\times \left([\alpha] - \frac{k^2}{\Lambda^2}[K] \right) \frac{k^2}{\Lambda^2} \begin{bmatrix} \tilde{\phi} \\ \tilde{\varphi} \end{bmatrix}_k + (\zeta^A)^{-2} [\tilde{A} \quad \tilde{a}]_{-k}^m$$
$$\left. \times \left([\alpha] - \frac{k^2}{\Lambda^2}[\mu] \right) \left(\frac{k^2}{\Lambda^2} \delta^{mn} - \frac{k^m k^n}{\Lambda^2} \right) \begin{bmatrix} \tilde{A} \\ \tilde{a} \end{bmatrix}_k^n \right\}. \tag{87}$$

Graphs are always evaluated at $k^2 \approx \Lambda^2$. Because longitudinal excitations are assumed dominated by $[K]$, scale invariance of graphs is maintained by constructing $[K]$ to be classically marginal. If $\mu = 0$, however, classical scaling of A, a is controlled by the density term $[\alpha]$. This remains classically marginal if a "separate" $[\alpha]^A$ from the compressional $[\alpha]$ matrix is associated with the $[A \quad a]$ fields, and the scaling of Eq. (56) replaced with

$$[\alpha]^A \to [\alpha]^A + [\delta\alpha]^A. \tag{88}$$

The induced scaling of longitudinal fields is as before:

$$\zeta^\phi \to \left(1 + \frac{\delta\Lambda}{\Lambda} \right)^{d/2+2} \zeta^\phi, \tag{89}$$

while that for shear is

$$\zeta^A \to \left(1 + \frac{\delta\Lambda}{\Lambda} \right)^{d/2+1} \zeta^A. \tag{90}$$

Scattering vertices likewise must be scaled differently, according to the number of compressional and shear fields they couple. Because displacements are related to compressional and shear potentials by the same number of spatial derivatives, the wave number contribution to the dimensionality of density-driven scattering interactions involving shear is the same as in Eq. (47). If one considers a term coupling $\phi^q A^{4-q}$ fields, and denotes its nondimensionalized coefficient Γ^q, it follows that $\Gamma^q (\zeta^\phi/\zeta^A)^{4-q}$ must have q-independent scaling under the sequence of transformations leading from Eq. (50) to Eq. (53). Then, from the results (53), (88), and (90),

$$\Gamma^q \to \left(1 + \frac{\delta\Lambda}{\Lambda} \right)^{q-d} \Gamma^q + \delta\Gamma^q. \tag{91}$$

Only the all-compressional (ϕ^4) sector in $d=3$ is classically relevant, and vertices with one shear excitation are classically marginal. All other shear interactions are classically irrelevant. From Eqs. (54) and (55), it follows that all shear interactions, like the compressional sector, are irrelevant for nondensity-driven scattering.

The vertices contributing to renormalization of the relevant interaction are shown in Fig. 6. The very assumption that (in the sense of the relevant eigenvalues) $[K] \gg [\alpha]$, used in evaluating the compressional sector, implies that vertices involving the transverse Green's function dominate near the natural scale as $[\alpha]^{-1} \gg [K]^{-1}$. The comparison of Eqs.

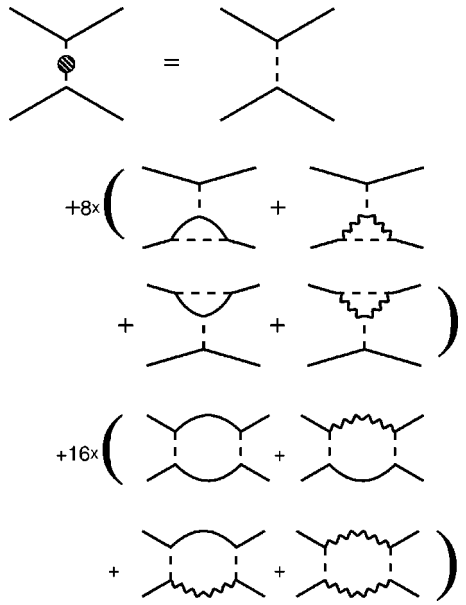

FIG. 6. Diagrams renormalizing the all-scalar interaction vertex. Only the box graphs involving single shear propagators (wavy lines) are classically marginal. All other graphs involving shear are classically irrelevant. Penguin graphs generate only wave number contractions respecting the replica structure, while box graphs also generate isotropic contractions at $\mathcal{O}(1/d^2)$.

(85) and (86) shows that if classical scaling were the only consideration, the power-law suppression of vertices would compensate for the different initial magnitudes at $[\alpha]\sim[K]$, which is of course where the roots lie and this evaluation must be replaced with the sigma-model renormalization of Ref. 3.

In Fig. 6, however, perturbative enhancements are amplified by classical scaling in the ϕ^4 vertex, whereas they are not enhanced in the similar graph expansions with one or more external shear legs. There thus exists the possibility of a perturbative range where the scalar-only graphs gradually come to dominate even though $[\alpha]^{-1}\geqslant[K]^{-1}$. If this happens sufficiently early in the RG flow over a large range of scales, the characteristics of the naive poroacoustic limit will be recovered.

The classical suppression of vertices higher order in shear makes it possible to approximate all shear vertices in Fig. 6 by their classically-scaled forms, which can be evaluated in closed form at least in a neighborhood of the natural scale. This evaluation, though less complete than was possible for the naive poroacoustic limit, indicates the form of stationary rays selected by the flow, and provides a starting point for analysis of the nontrivial shear sector.

Introducing a notation for the components of $[\alpha]$,

$$[\alpha]\equiv\begin{bmatrix}\alpha_\rho & -\alpha_f\\ -\alpha_f & \alpha_m\end{bmatrix}, \tag{92}$$

the small-shear limit is defined as $\mu\alpha_m/|\alpha|\to 0$. Recalling that $k^2\approx\Lambda^2$ in RG graphs, the shear propagator appearing in Eq. (43) becomes

$$([\mu]-[\alpha])^{-1}\to-[\alpha]^{-1}-\frac{\mu}{|\alpha|^2}\begin{bmatrix}\alpha_m\\ \alpha_f\end{bmatrix}[\alpha_m\quad\alpha_f]+\ldots \tag{93}$$

(with the second term kept mostly for the interesting fact that it is degenerate, like $[\mu]$).

Defining an abbreviated notation for inverses of kernels, $[K-\alpha]\equiv([K]-[\alpha])$, $[\mu-\alpha]\equiv([\mu]-[\alpha])$, and this time keeping terms of $\mathcal{O}(\alpha)$, the graphs of Fig. 6 may be evaluated, starting from the bare form. In bare vertices, only wave number contractions respecting the replica pairing appear. The contribution of box and penguin diagrams to this replica-preserving sector is written as in Eq. (62)

$$\begin{aligned}\delta\Gamma_{\alpha\beta}\sigma^\alpha_{ab}\sigma^\beta_{cd}=\frac{16}{2\pi^2}\Gamma_{\alpha\beta}\Gamma_{\gamma\delta}\Bigg\{\frac{1}{2}\Bigg[\sigma^\alpha_{ab}\Bigg(\frac{1}{d}\sigma^\gamma[K-\alpha]^{-1}\sigma^\beta[K-\alpha]^{-1}\sigma^\delta+\Big(1-\frac{1}{d}\Big)\sigma^\gamma[\mu-\alpha]^{-1}\sigma^\beta[\mu-\alpha]^{-1}\sigma^\delta\Bigg)_{cd}\\ +\Bigg(\frac{1}{d}\sigma^\alpha[K-\alpha]^{-1}\sigma^\gamma[K-\alpha]^{-1}\sigma^\beta+\Big(1-\frac{1}{d}\Big)\sigma^\alpha[\mu-\alpha]^{-1}\sigma^\gamma[\mu-\alpha]^{-1}\sigma^\beta\Bigg)_{ab}\sigma^\delta_{cd}\Bigg]\\ +\Big(1-\frac{2}{d}\Big)(\sigma^\alpha[\mu-\alpha]^{-1}\sigma^\gamma)_{ab}(\sigma^\delta[\mu-\alpha]^{-1}\sigma^\beta)_{cd}+\frac{1}{d}[(\sigma^\alpha[\mu-\alpha]^{-1}\sigma^\gamma)_{ab}(\sigma^\delta[K-\alpha]^{-1}\sigma^\beta)_{cd}\\ +(\sigma^\alpha[K-\alpha]^{-1}\sigma^\gamma)_{ab}(\sigma^\delta[\mu-\alpha]^{-1}\sigma^\beta)_{cd}]\Bigg\}\frac{\delta\Lambda}{\Lambda}.\end{aligned} \tag{94}$$

Only the box diagrams contribute contractions violating the replica pairing, and the counterpart to Eq. (63) (starting at $\xi=0$) becomes

$$\delta(\xi\Gamma_{\alpha\beta})\sigma^\alpha_{ab}\sigma^\beta_{cd}=\frac{16}{2\pi^2}\frac{\Gamma_{\alpha\beta}\Gamma_{\gamma\delta}}{d(d+2)}(\sigma^\alpha([\mu-\alpha]^{-1}-[K-\alpha]^{-1})\sigma^\gamma)_{ab}(\sigma^\delta([\mu-\alpha]^{-1}-[K-\alpha]^{-1})\sigma^\beta)_{cd}\frac{\delta\Lambda}{\Lambda}. \tag{95}$$

The dimension d has been kept explicit in Eqs. (94) and (95), because replica-violating terms are generated at $\mathcal{O}(1/d^2)$, while Γ grows at $\mathcal{O}(1/d)$ for compression, and $\mathcal{O}(1)$ for shear. Any stationary ratio ξ^* of replica-violating terms must therefore have $\xi^* \sim \mathcal{O}(1/d)$ or $\xi^* \sim \mathcal{O}(1/d^2)$, depending on which sector dominates the RG, so $1/d$ is a regulator preserving the wave vector structure of the bare interaction. Large d formally allows the nonrespecting terms to be ignored, though the qualitative behavior of the RG flow is not expected to differ at finite ξ, as in the naive poroacoustic limit it did not.

At $\mu \to 0$, $d \geqslant 2$, and $[\alpha]^{-1} \gg [K]^{-1}$, Eq. (94) is positive-definite, indicating that RG flow is toward strong coupling, qualitatively as in the naive limit. The sign becomes uncertain near $[\alpha] \sim [K]$, because of cross terms in $[\alpha]$ and $[K]$, but this is also the region where the positive-definite scalar-only graphs are expected to start to dominate. Thus, while it is not possible to make universal statements about the proper poroacoustic RG flow, it does not look like general parameters will lead to nontrivial fixed points. Rather, an initial $[\alpha]$-driven flow toward strong coupling should either include the whole range above the experimental scale, or lead into a subsequent $[K]$-driven flow that enhances scattering of the slow wave, as in the naive analysis.

C. Inversion at finite shear modulus

Scattering in the full Biot theory at finite μ is in general very complicated. The problem is not so much the single-scattering process, which has been considered even for finite-sized obstacles,[24,32] as that iteration generates an RG flow with multiple intertwined behaviors. Even scattering induced by density fluctuations alone leads to all possible wave number and polarization contractions consistent with transversality of the shear potentials. Unless there is some simplifying restriction on the initial form of the scattering operator, it is also not generally possible to isolate a single scaling dimension for shear fields that provides a natural separation of classical and anomalous scaling, because of the degeneracy of the shear modulus matrix. However, the form of the shear propagator at $[\mu] \sim [K] \gg [\alpha]$ is interesting, and suggests that some features of the poroacoustic limit may yet remain.

The large-shear limit, defined by $\mu \alpha_m / |\alpha| \to \infty$, produces the inverse kernel

$$([\mu]-[\alpha])^{-1} \to -\frac{1}{\alpha_m}\begin{bmatrix} 0 & \\ & 1 \end{bmatrix} + \frac{1}{\mu \alpha_m^2}\begin{bmatrix} \alpha_m \\ \alpha_f \end{bmatrix}[\alpha_m \quad \alpha_f] + \ldots . \tag{96}$$

The first term on the right-hand side of Eq. (96) scales classically as $[\alpha]^{-1}$, while the second scales as $\mu^{-1}[\alpha]^0$. Thus, the appropriate classical scaling of transverse fields can depend on which terms from Eq. (96) have nonzero projection under the scattering operator. Section VIII will focus on examples where the poroacoustic scaling can be used because the scattering vertex couples only to the first term in Eq. (96).

In the more general case, since two out of three matrix elements in the shear Green's function are controlled by μ, the best one can do may be to revert scaling of A, a to the same as that for ϕ:

$$\zeta^A \to \left(1 + \frac{\delta\Lambda}{\Lambda}\right)^{d/2+2} \zeta^A, \tag{97}$$

while $[\alpha]$ returns to the scaling of Eq. (56). Formally, this makes all density fluctuation-induced scattering terms relevant, though the scaling of $[\alpha]$ in Green's functions causes corrections involving the first term in Eq. (96) to have fixed magnitude in successive RG iterations. Qualitatively, the RG flow near the natural scale should resemble that of the poroacoustic limit, but with Eq. (96) replacing Eq. (93) in Eqs. (94) and (95).

The interesting feature of the large-shear limit is that the first term in Eq. (96) focuses scattering on the fluid-fluid Green's function. The strongest stationary ray selected by this term, by inspection, is

$$\sigma^*_{\mu \to \infty} \equiv \begin{bmatrix} 0 & \\ & 1 \end{bmatrix}. \tag{98}$$

This matrix couples entirely to fluid, so it will generally scatter the slow wave more strongly than the fast, since the former generally involves a larger component of fluid motion. Dominance of this term may thus lead qualitatively to the same phenomenon that will be achieved by choice of the source of scattering in the examples below: an $[\alpha]$-driven early RG that couples smoothly to a later $[K]$-driven flow near the stationary ray of Sec. VI.

D. Fluid inertia and wave function renormalization

Renormalization corrections in simple elasticity (at finite shear) generically reduce the effective sound speed, qualitatively because they increase the average path length by scattering. The sign of the first term in Eq. (96), by contrast, may be expected to *reduce* the eigenvalues of $[\alpha]$, thus leading to increased sound speeds. Further, vanishing fluid shear modulus implies zero propagation distance, so a qualitative understanding in terms of changed path length makes no sense.

The physical basis of the $[\alpha]$-driven renormalization near the natural scale may be understood by computing the first perturbative correction below Λ_0 (where the interactions are still simple), and then performing a wave function renormalization to leave the form of $[\alpha]$ invariant, as in naive poroacoustic scaling. This is reasonable, because although classical scaling forbids assigning a single dimension to shear fields, it does not significantly impact the early perturbative iterations.

The extension of Eq. (60) to include shear, at $\xi = 0$ and using $d = 3$ to simplify prefactors, is

$$[\delta\alpha]=-\frac{8}{2\pi^2}\Gamma_{\alpha\beta}\sigma^{\alpha}\left\{\left(1-\frac{1}{d}\right)\frac{1}{\alpha_m}\begin{bmatrix}0 & \\ & 1\end{bmatrix}-\left(1-\frac{1}{d}\right)\frac{1}{\mu\alpha_m^2}\begin{bmatrix}\alpha_m\\ \alpha_f\end{bmatrix}[\alpha_m \quad \alpha_f]-\frac{1}{d}[K]^{-1}\right\}\sigma^{\beta}\frac{\delta\Lambda}{\Lambda}. \tag{99}$$

d has been left explicit as in Eqs. (94) and (95), to show which terms survive as $\xi^*\sim 1/d\to 0$. The correction to $[\alpha]$ for transverse waves replaces $(1-1/d)$ with $2/d$ in Eq. (99). In the particular case $d=3$, this admits a homogeneous renormalization of scalar and vector potentials, which will be exploited below in physical interpretations. In formally large d, transverse $[\alpha]$ does not renormalize, but corrects the compressional dispersion relation in fixed form, causing the effective dispersion to depend only on the renormalization of the effective interaction vertex.

Again considering stationary solutions (64) for simplicity, along the maximal ray (98), the leading density correction becomes (using $d=3$)

$$[\delta\alpha]\to-\frac{8}{3\pi^2}\frac{\Gamma}{\alpha_m}\begin{bmatrix}0 & \\ & 1\end{bmatrix}\frac{\delta\Lambda}{\Lambda}. \tag{100}$$

Redimensionalized, the only fractional correction is to the component m, and will be denoted

$$\eta\equiv\frac{\delta m}{m}=-\frac{8\pi}{3}\left(\frac{G_0}{l_0^d m^2}\right)\frac{\delta\Lambda}{\Lambda}. \tag{101}$$

The kinetic term in the free action, which dominates the transverse propagator at this scale, may be returned to canonical form, while preserving the definition of the relative fluid displacement in terms of an effective porosity, by demanding that

$$\begin{aligned}&[\dot u \quad \dot U]\begin{bmatrix}1 & \beta\\ 0 & -\beta\end{bmatrix}\\ &\quad\times\begin{bmatrix}\rho & -\rho_f\\ -\rho_f & m+\eta m\end{bmatrix}\begin{bmatrix}1 & 0\\ \beta & -\beta\end{bmatrix}\begin{bmatrix}\dot u\\ \dot U\end{bmatrix}\\ &\quad\equiv[\dot{\tilde u} \quad \dot{\tilde U}]\begin{bmatrix}1 & \tilde\beta\\ 0 & -\tilde\beta\end{bmatrix}\begin{bmatrix}\rho & -\rho_f\\ -\rho_f & m\end{bmatrix}\begin{bmatrix}1 & 0\\ \tilde\beta & -\tilde\beta\end{bmatrix}\begin{bmatrix}\dot{\tilde u}\\ \dot{\tilde U}\end{bmatrix}.\end{aligned} \tag{102}$$

The required rescalings of displacement fields are

$$\tilde u=\left(1+\frac{\eta}{2}\frac{\rho_f^2}{|\rho|}\right)u, \tag{103}$$

$$\tilde U=\left(1-\frac{\eta}{2}\frac{(1-\beta)}{\beta}\frac{\rho_f\rho_r}{|\rho|}\right)U, \tag{104}$$

and the effective porosity becomes

$$\tilde\beta=\left\{1+\frac{\eta}{2}\left[1+\frac{(1-\beta)}{\beta}\frac{\rho_f\rho_r}{|\rho|}\right]\right\}\beta. \tag{105}$$

The relation (7) may be preserved in terms of the new effective porosity, too, by defining

$$(1-\beta)\rho_r+\beta\rho_f\equiv(1-\tilde\beta)\tilde\rho_r+\tilde\beta\rho_f, \tag{106}$$

which gives the renormalized effective grain density

$$\tilde\rho_r=\rho_r-\frac{\beta-\tilde\beta}{1-\tilde\beta}(\rho_r-\rho_f). \tag{107}$$

The effect of fluid-controlled renormalization may be understood as an inertial confinement, somewhat resembling that proposed in Ref. 33. As $\eta<0$, $\tilde\beta<\beta$. After short wavelengths are integrated out, the effective grain density (107) therefore becomes an average of the bare grain and fluid densities, as if some fluid is now incorporated into the effective solid matrix. Furthermore, the diagonal component of solid self-inertia, obtained by multiplying the central matrices in Eq. (102), is less sensitive to ρ_f and m, because of smaller $\tilde\beta$. Thus the reduction in effective porosity does appear physical.

The reason such entrainment of fluid in the solid matrix arises from the transverse scattering corrections is that, at vanishing shear modulus, fluid shear relieves stresses by flowing around (or through) local regions of higher impedance, such as higher tortuosity. At nonvanishing frequency, such flow is inertially hindered, so part of the fluid can no longer move separately from the frame.

A consequence of this interpretation is that a new component of frame stress should be transmitted by the entrained fluid component, stiffening the effective moduli. Introducing the notation $\tilde w\equiv\tilde\beta(\tilde u-\tilde U)$ to return to Biot's canonical variables, the associated transverse potentials are renormalized by the same matrix as restores $[\rho]$ to canonical form:

$$[A \quad a]^m\begin{bmatrix}\mu & 0\\ 0 & 0\end{bmatrix}\begin{bmatrix}A\\ a\end{bmatrix}^n=[\tilde A \quad \tilde a]^m\begin{bmatrix}\tilde\mu & 0\\ 0 & 0\end{bmatrix}\begin{bmatrix}\tilde A\\ \tilde a\end{bmatrix}^n. \tag{108}$$

The importance of retaining the effective porosity matrix structure in Eq. (102) is that this defines the unique wave function renormalization preserving the *form* of the shear modulus matrix in Eq. (108), keeping $\tilde u$ the well-defined solid degree of freedom.

The resulting scaling of μ is

$$\tilde\mu=\left(1-\eta\frac{\rho_f^2}{|\rho|}\right)\mu. \tag{109}$$

Since, trivially, the shear modulus matrix is simply rescaled, the correction to the shear velocity is immediate from Fig. 4:

$$\tilde c_{sh}^2=c_{sh}^2\left(1-\eta\frac{\rho_f^2}{|\rho|}\right), \tag{110}$$

and indeed, $\tilde c_{sh}^2>c_{sh}^2$.

Renormalization of the compressional potentials defines the effective compressibility matrix:

$$[\phi \quad \varphi]\begin{bmatrix} H & -C \\ -C & M \end{bmatrix}\begin{bmatrix} \phi \\ \varphi \end{bmatrix} = [\tilde{\phi} \quad \tilde{\varphi}]\begin{bmatrix} \tilde{H} & -\tilde{C} \\ -\tilde{C} & \tilde{M} \end{bmatrix}\begin{bmatrix} \tilde{\phi} \\ \tilde{\varphi} \end{bmatrix}, \quad (111)$$

in which

$$\tilde{H} = H + \eta \frac{\rho_f(\rho C - \rho_f H)}{|\rho|}, \quad (112)$$

$$\tilde{C} = C - \frac{\eta}{2} \frac{\rho(mC - \rho_f M)}{|\rho|}, \quad (113)$$

$$\tilde{M} = M - \eta M, \quad (114)$$

and so

$$|\tilde{K}| = \left(1 - \eta \frac{\rho m}{|\rho|}\right)|K|. \quad (115)$$

To the extent that $[\rho]$ and $[K]$ are coplanar, as in the examples above, Eq. (115) implies that at least one of the compressional wave speeds must increase, because the product of the relevant modulus eigenvalues increases. Unlike the shear case, however, the independent impact of scaling on fast and slow wave speeds appears to depend on relative matrix coefficients, and cannot be inferred universally.

One interesting case that will appear below, however, involves nearly coplanar $[\rho]$ and $[K]$, with $2C \sim (H+M) \gg (H-M) \gg (M-C)$. An analysis of the effects on Fig. 5, together with Eqs. (112)–(114), gives

$$\tilde{c}_f^2 \approx c_f^2 \left(1 - \frac{\eta}{2} \frac{\rho(m - \rho_f)}{|\rho|}\right) \quad (116)$$

and

$$\tilde{c}_s^2 \approx c_s^2 \left(1 - \eta \frac{\rho_f^2}{|\rho|}\right). \quad (117)$$

Equation (116) is probably qualitatively robust, as it results from a homogeneous scaling of both eigenvalues, and the transverse piercing of the upper light cone, analogously to the shear case. Equation (117) is less obviously so, because it involves the interplay of a rescaling, and an angle change that renders $[K]$ more or less null. Since the slow wave speed is a sensitive function of the sliver angle between $[K]$ and the light cone, the combined influence of scaling and angle changes is not obviously universal. A general increase in the fast wave speed, however, would be expected from the entrainment arguments above.

VIII. EXAMPLES

There is a wide variety of possible relations between the longitudinal and transverse Biot wave equations, so it was impossible in the preceding sections to derive the transitional behaviors of RG flows affected by both, in any general form. Two examples will be developed here, for different ''typical'' Biot parameter sets, to show how the pieces of the previous discussion fit together. In both examples, tortuosity fluctuations will be chosen as the source of scattering, because this leads to poroacoustic classical scaling independently of the value of the shear modulus, removing the need to renormalize the whole transverse scattering sector.

TABLE I. Parameters for Ridgefield Sandstone (from Ref. 20). l_0 was chosen as grain size from Ref. 14, which is roughly ten times the dynamically connected pore size (Ref. 20).

l_0	200 μm
β	0.366
K_r	4.99×10^{10} Pa
K_b	5.24×10^{9} Pa
μ	3.26×10^{9} Pa
ρ_r	2.48 g/cm^3
α_∞	1.58

The first example, liquid ^{4}He in a sintered glass bead pack, is intended as a realistic laboratory application of these results. The inviscid approximation can be made arbitrarily good, and the system lies near a ''rigid-frame'' limit, in which the Biot equations reduce to a scalar acoustic problem. The fluid-inertial ''stiffening'' of the last section will be clearly seen, and its frequency dependence is derived as a diagnostic for the magnitude of tortuosity fluctuations in the medium. In this example, the transition to naive poroacoustic scaling will not be seen within valid perturbation theory, so growth of the effective coupling will never significantly reduce the slow wave speed.

The second example uses parameters for naturally occurring water-saturated sediments, but ignores the real viscosity of water. This model was chosen because it has a shear wave even slower than the Biot slow wave, and thus admits a weak-shear limit near the end of the RG flow. The change in form of the transverse propagator in this range leads to decoupling from the slow-wave dispersion not seen in the last example, suggesting that naive poroacoustic scaling may be recovered in the late stages of this RG flow. Because viscosity is ignored, though, the results at best place upper bounds on the importance of coherence effects, which may have some relevance at very short wavelengths.

A. A rigid-frame limit

The obvious direct application of the inviscid RG is to superfluid^{4}He (He II). The fluid excitations extending bulk first and second sound to porous media have been studied both theoretically[15] and experimentally[14] in the rigid-frame limit, with excellent agreement. Because the normal fluid fraction is less than 1% and decaying as T^4 below 1.2 K, second sound modes may be excluded, and He II described as an inviscid simple fluid, to arbitrary accuracy, at suitably low but readily achievable temperatures.

Parameters for the solid matrix corresponding to sintered glass beads (Ridgefield Sandstone) are shown in Table I.[14,20] The fluid compressibility and density vary with temperature

along the saturated vapor pressure (SVP) line,[34] but bulk first sound speed is bounded above by ~ 238 m/s, giving $K_f \ll K_r$ at all temperatures. The expressions (9)–(12) then give $H > \mu \gg C \sim M$, so that for practical purposes $K_- = M = K_f/\beta$,

$$(v_- v_-^{\mathrm{T}}) \approx \begin{bmatrix} 0 & \\ & 1 \end{bmatrix}, \tag{118}$$

and the diagonalization of the wave equation is dominated by $[K]$ at all frequencies and gives $\rho_- = m = \alpha_\infty \rho_f/\beta$.

In the absence of viscosity, α_∞ is the tortuosity at all frequencies, and the most important parameter for scattering of slow waves. If tortuosity alone is varied in the underlying medium, the only matrix component of the scattering vertex becomes the dominant stationary ray of Eq. (98). In such a medium, the only component of the transverse propagator scattered at *any* μ is the first term in Eq. (96), and the poroacoustic scalings of Eqs. (88)–(91), which leave $[\alpha]$ classically invariant, are the correct ones to use. While for spherical grains tortuosity is a function of porosity, it will be assumed here that by appropriate variations of grain shape and arrangement, α_∞ has been varied at constant β, to achieve this simplification. (The next example shows that even if the origin of tortuosity fluctuations is taken to be porosity change, this is not a bad approximation.)

In the limit thus adopted, Biot theory reduces to a scalar acoustic theory, with nondimensionalized scattering strength at the natural scale defined as in Eq. (38), with $G_0/(l_0^d m_0^2) = \overline{(\delta m/m_0)^2} = \overline{(\delta \alpha_\infty/\alpha_{\infty 0})^2}$. The RG flow defines distinct effective longitudinal and transverse densities α_m^ϕ and α_m^A, renormalized by Eq. (56) and Eq. (88) respectively. There are five dimensionless couplings Γ^q, $q \in \{0, \ldots, 4\}$, renormalized by Eq. (91), of which only Γ^4 is classically relevant. Since irrelevant scaling suppresses perturbative corrections,

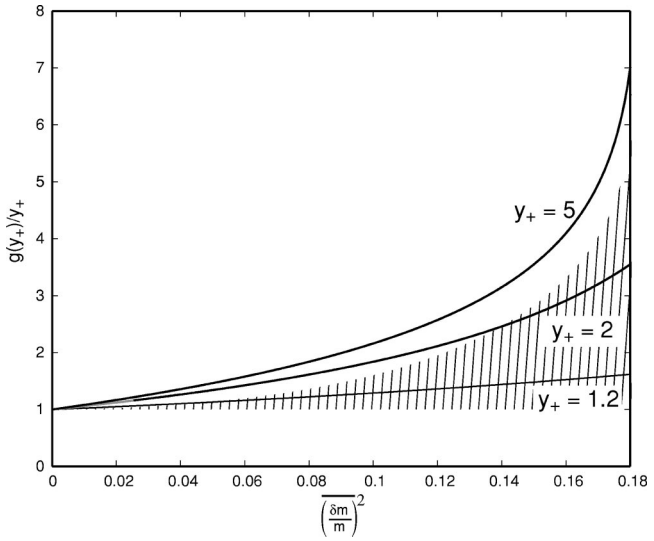

FIG. 7. $G^{\mathrm{eff}}(\Lambda)/G_0$ versus $\overline{(\delta m/m_0)^2}$, at $\Lambda_0/\Lambda = \lambda_{s0}(\omega)/l_0$. Hatched area, corresponding to strong coupling, is obtained from Fig. 9.

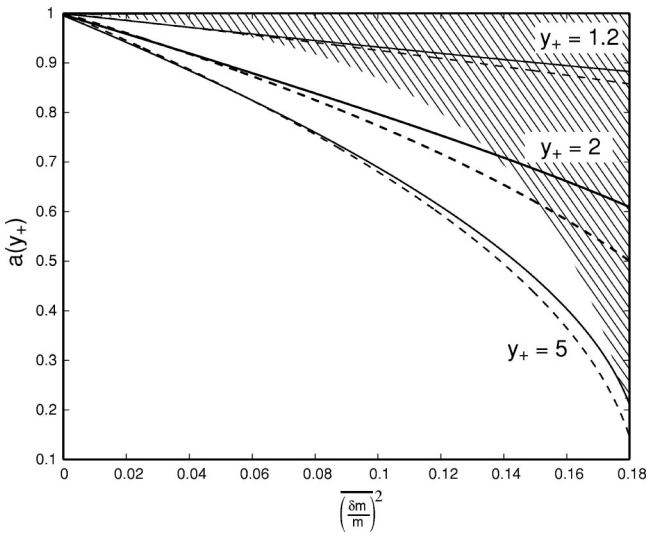

FIG. 8. Effective tortuosities $m^{\mathrm{eff}}(\Lambda)/m_0$ at $\Lambda_0/\Lambda = \lambda_{s0}(\omega)/l_0$, for differently renormalized ϕ (solid) and A (dash) sectors. Hatched region corresponds to strong coupling.

for all $q \in \{0, \ldots, 3\}$ the classical form $\Gamma^q(\Lambda) = (\Lambda/\Lambda_0)^{q-d}\Gamma_0$ will be used in RG flows.

The simplest quantities to evaluate as a function of renormalization scale Λ are then

$$g \equiv \frac{\Gamma^4}{\Gamma_0}; \quad a^\phi \equiv \frac{\alpha_m^\phi}{\alpha_{m0}}; \quad a^A \equiv \frac{\alpha_m^A}{\alpha_{m0}}. \tag{119}$$

In $d=3$, the convenient measure of bare coupling strength is $\varepsilon \equiv (8\pi/3) G_0/(l_0^d m_0^2)$. If the range of renormalization is denoted $y \equiv \Lambda_0/\Lambda$, RG flows are integrated from $y \in (1, y_+)$, where (as long as the effective density is not renormalized by more than order unity), $y_+ \approx \Lambda_0 c_{s0}(\omega)/\omega = \lambda_{s0}(\omega)/l_0$, and $\lambda_{s0}(\omega)$ is the unrenormalized slow wavelength at frequency ω. In terms of these quantities, the perturbative correction (94) (approximating $\xi = 0$ as discussed above) gives for g

$$\frac{dg}{d\log y} = g + \varepsilon\left[\frac{3}{(a^A y)^2} - \frac{2}{a^A y_+^2} + \frac{g^2}{y_+^4}\right]. \tag{120}$$

The corresponding equations for a^ϕ, a^A, from Eq. (99), are

$$\frac{da^A}{d\log y} = -\varepsilon\left[\frac{1}{a^A y^3} - \frac{1}{2 y y_+^2}\right], \tag{121}$$

$$\frac{da^\phi}{d\log y} = 2a^\phi - \varepsilon\left[\frac{1}{a^A y} - \frac{g}{2y_+^2}\right]. \tag{122}$$

The ratio $g(y_+)/y_+$ obtained from Eqs. (120)–(122) by numerical integration is shown in Fig. 7 as a function of $\overline{(\delta m/m_0)^2}$, for several values of renormalization scale y_+. This is the quantity G^{eff}/G_0, for G^{eff} as defined in Eq. (70). Thus the first claim of the paper can clearly be seen: the resumming of perturbation theory, by renormalization from the natural scale to a neighborhood of the on-shell wave

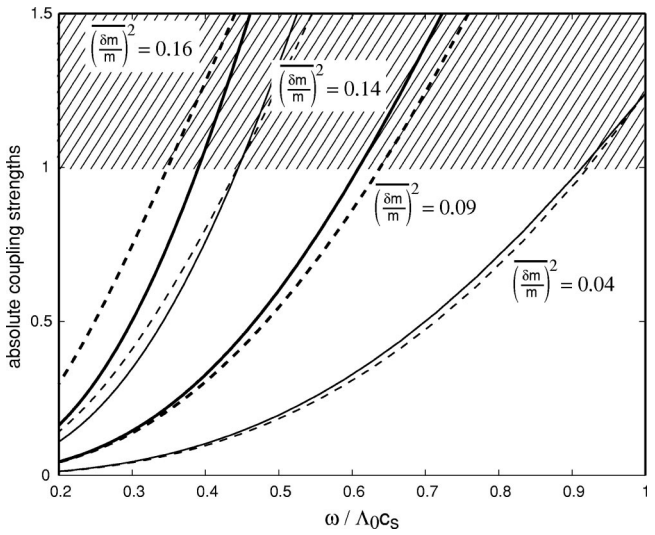

FIG. 9. Longitudinal (solid) and transverse (dash) absolute coupling strengths, respectively Γ^4/K_-^2 and $\Gamma^0/(\alpha_m^A)^2$, versus $\omega/\Lambda_0 c_{s0}(\omega)$, at several values of $\overline{(\delta m/m_0)^2}$. Values $\geqslant 1$ define strong coupling, and the hatched region in this figure maps to that in all other plots.

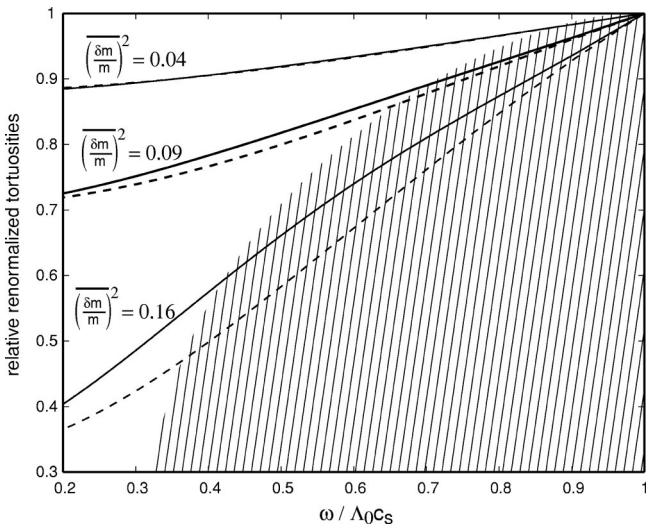

FIG. 10. ϕ (solid) and A (dash) normalized effective tortuosity $m^{\text{eff}}(\Lambda)/m_0$ versus $\omega/\Lambda_0 c_s(\omega)$, at several values of $\overline{(\delta m/m_0)^2}$. Hatched region represents strong coupling.

number, can give an effective scattering vertex significantly larger than the Born-approximation value G_0. First-order perturbation theory becomes invalid in the hatched region of Fig. 7 (obtained by rearranging Fig. 9 below), due to high-frequency growth of the bare Rayleigh cross section. However, it is clear that the greatest renormalization enhancements occur at large $\overline{(\delta m/m_0)^2}$, where strong coupling is reached at freqiuencies well below the natural scale (e.g., the $y_+ = 5$ curve.)

A similar plot of the effective longitudinal and transverse tortuosities, normalized by their initial values, is given in Fig. 8. Under all conditions shown here, both effective tortuosities are renormalized downward, leading to *increases* in effective sound speed relative to the bare value. This is an example of the fluid-inertia-induced ''stiffening'' described in Sec. VII D.

All terms in square brackets in Eq. (120) remain positive for all values of a^A generated by this flow, verifying that the coupling is never weakened during a transition from *a*-dominated to *g*-dominated flow. It is possible to choose large enough $\overline{(\delta m/m_0)^2}$ to cause the *g* term in Eq. (122) to eventually dominate, leading formally to the large-*y reduction* of the longitudinal slow wave speed described in Eq. (81). However, this effect does not appear to lie within the range of validity of this perturbation expansion for this model, because large coupling always sets in first.

The coupling strengths Γ^4/K_-^2 of Eq. (85) and Γ^0/α_m^2 of Eq. (86) are plotted versus naturally scaled frequency in Fig. 10, at several values of $\overline{(\delta m/m_0)^2}$. The frequency dependence of the bare Rayleigh cross section can be clearly seen, as strong coupling is encountered at progressively lower frequencies for greater heterogeneities. The weakest variance at which strong coupling is achieved below the natural scale is $\overline{(\delta m/m_0)^2} \sim 0.04$, as predicted by purely classical scaling in Eq. (84).

Figure 9 also shows that there is limit of $\overline{(\delta m/m_0)^2} \lesssim 0.14$ for validity the perturbation theory assumed here. For greater heterogeneity, scattering operators between transverse excitations become strong before those for longitudinal, and transverse-excitation propagation cannot be assumed to take the perturbative form giving Eq. (94). (This range of validity still corresponds to relative standard deviations up to $\sim 40\%$ in α_∞.)

Finally, Fig. 10 shows renormalized tortuosity versus frequency at relative standard deviations of 20%, 30%, and 40% in α_∞. The coherence effects from scattering into transverse excitations, which increase with heterogeneity, are less severe with increasing frequency due to the shorter renormalization range. This appears as a roughly linear slowing of c_s with increased frequency at small heterogeneities [say $\delta c_s/c_{s0} \approx 5\%$ for 20% standard deviation and $\omega/2\pi \in (0.2-1)\times c_{s0}/l_0$].

It is clear from these plots that gross deviations from homogeneous Biot theory are not predicted for moderate heterogeneities and low frequencies. The largest determinant of strong coupling is still the frequency dependence of the bare Rayleigh scattering cross section, and even for standard deviations in relative tortuosity fluctuations $\sim 20\%$, strong coupling is not encountered until the slow wavelength is comparable to the grain size. However, there is a predicted $\sim$linear decrease of slow wave speed with frequency, with coefficient proportional to the variance in tortuosity, which is qualitatively distinct from the usual Biot dispersion due to viscous effects. Thus, He II can be used not only to derive mean effective-medium parameters as in Ref. 14, but also to estimate their fluctuations by measuring dispersion in the inviscid limit.

B. A weak-frame limit

An example of a weak-frame Biot model is the description by Stoll and Kan[18] of water-saturated ''unconsolidated''

TABLE II. Parameters for water-saturated quartz sands (from Ref. 18). l_0 was chosen as grain size, and tortuosity α_∞ corresponds to their ''virtual mass constant'' c.

l_0	200 μm
β	0.47
K_r	3.6×10^{10} Pa
K_b	4.36×10^{7} Pa
K_f	2.0×10^{9} Pa
μ	2.61×10^{7} Pa
ρ_r	2.65 g/cm^3
ρ_f	1.0 g/cm^3
α_∞	1.25

quartz sands. Grain size is comparable to the Ridgefield Sandstone of the last example, and their best-fit modulus and density parameters are given in Table II. K_b and μ, though much smaller than in the last example, are still large enough that the frame behaves acoustically as if it had some measure of consolidation. Further, unrenormalized $k_{sh}^2\approx 2k_s^2$ at any ω, giving a modest weak-shear condition

$$\frac{\mu\alpha_m}{|\alpha|}=\frac{\Lambda^2}{k_{sh}^2(\omega)}<1 \tag{123}$$

as Λ approaches $k_s^2(\omega)$ in RG flows.

Because both slow and shear wave speeds are determined by frame compressibility in this example, the structure of the Biot matrices remains important to the RG flow, and gives rise to interesting decoupling effects. These are most easily seen using the decomposition of Sec. VI.

From Table II and Eqs. (7) and (8), $\rho=1875$ kg/m^3 and $m=2660$ kg/m^3, and the dyadic decomposition of $[\rho_0]$ is

$$[\rho_0]\equiv\frac{\rho_+}{2}(\sigma^0+\sigma_\rho^L)+\frac{\rho_-}{2}(\sigma^0-\sigma_\rho^L), \tag{124}$$

with eigenvalues $\rho_+=3341$ kg/m^3 and $\rho_-=1193$ kg/m^3. The longitudinal matrix σ_ρ^L is related to the basis (32) as

$$\sigma_\rho^L=-\sin\theta_\rho\sigma^1+\cos\theta_\rho\sigma^2, \tag{125}$$

with an angle $\theta_\rho=0.619\pi$.

Using the relations (9)–(12), $H=4.073\times10^9$ Pa, $C=4.000\times10^9$ Pa, $M=4.005\times10^9$ Pa, and $\mu=2.6\times10^7$ Pa, and as assumed at the end of Sec. VII D, $2C\approx H+M\gg H-M\gg M-C$. A decomposition of $[K_0]$ as in Eq. (124) gives

$$[K_0]\equiv\frac{K_+}{2}(\sigma^0+\sigma_K^L)+\frac{K_-}{2}(\sigma^0-\sigma_K^L), \tag{126}$$

where $K_+=8.039\times10^9$ Pa, $K_-=3.849\times10^7$ Pa,

$$\sigma_K^L=-\sin\theta_K\sigma^1+\cos\theta_K\sigma^2, \tag{127}$$

and $\theta_K=0.497\pi$.

$K_+/K_-\gg\rho_+/\rho_-$, so like the last example, this model is strongly ''natural'' in the sense of Sec. VI. Further, $[\rho_0]$ and $[K_0]$ are nearly coplanar, and $\theta_\rho-\theta_K=0.122\pi$ is a small angle that will be ignorable in the approximate discussion below. In the same notation, the shear modulus matrix is nearly orthogonal to the entire compressional kernel, with $\theta_{sh}\equiv0$. This vector decomposition, shown in Fig. 4, is the feature responsible for shear decoupling.

Mostly to show how it works, in this example porosity change will be assumed responsible for tortuosity fluctuations. In a model by Berryman,[35] the tortuosity and porosity are related as

$$\alpha_\infty\equiv1+r\left(\frac{1}{\beta}-1\right). \tag{128}$$

For the parameters quoted here, $r\approx0.22$, while for spheres $r=0.5$ is predicted. Variation of $[\rho]$ with porosity gives

$$\frac{\partial[\rho]}{\partial\log\beta}\equiv-\begin{bmatrix}\rho_r-\rho & \\ & \dfrac{m-\rho_f}{1-\beta}\end{bmatrix}, \tag{129}$$

in which $\rho_r-\rho=776$ kg/m^3 and $(m-\rho_f)/(1-\beta)=3131$ kg/m^3. Thus, approximating $\Gamma_{\alpha\beta}$ by the form in Eq. (64), with σ^* as in Eq. (98), omits terms roughly 25% as large as those kept. That approximation will be made here to justify the poroacoustic scaling relation in the range of Λ not satisfying Eq. (123), because the matrix (98) couples only to the first term in Eq. (96).

The coupling strength corresponding to Eq. (86) is

$$\frac{\Gamma}{\alpha_m^2}=\pi^3\overline{(\delta\log\beta)^2}\left(\frac{1-\rho_f/m}{1-\beta}\right)^2\left(\frac{\Lambda}{\Lambda_0}\right)^3, \tag{130}$$

so strong coupling within the homogenization regime is classically predicted to require $\overline{(\delta\log\beta)^2}\geqslant0.03$ with these parameters.

Defining $\sigma_{\pm K}\equiv(\sigma^0\pm\sigma_K^L)/2$, and using the fact that θ_K differs from $\pi/2$ by a fraction of a percent to approximate

$$\sigma_{\pm K}\approx\frac{1}{2}\begin{bmatrix}1 & \mp1\\ \mp1 & 1\end{bmatrix}, \tag{131}$$

it follows that $\sigma^*\sigma_K^T\sigma^*=0$. The determinant of the compressional kernel $[K-\alpha]$ differs from that for purely coplanar $[K]$ and $[\alpha]$ by terms of $\mathcal{O}((\theta_\rho-\theta_K)^2)$. Since this difference angle appears linearly only as the coefficient of a matrix (σ_K^T) projected to zero by σ^*, it can simply be ignored, and $[K]$ and $[\alpha]$ treated as coplanar, at the level of approximation made here.

Ignoring perturbative corrections to $[\alpha]$ (which is classically marginal under poroacoustic scaling) and terms of $\mathcal{O}(K_-/K_+)$, and using $\sigma^*=\sigma^*\sigma^*\sigma^*=2\sigma^*\sigma_{\pm K}\sigma^*$, the compressional projectors in Eq. (94) evaluate to

$$\sigma^*[K-\alpha]^{-1}\sigma^*=\frac{1}{(1-k_s^2/\Lambda^2)}\left(\frac{\sigma^*}{2K_-}\right). \tag{132}$$

In the large-Λ (large-shear) range, the transverse propagators have the same form as in the last example, and the only difference in the RG flow is the factor of two in Eq.

(132). However, for $\Lambda \lesssim \sqrt{2}k_s(\omega)$, both of $\sigma_{\pm K}$ must be kept in evaluating $[\alpha]^{-1}$ in Eq. (93), along with the fact that $\rho_-/\rho_+ \approx 1/3$ and $2\rho_-/m \approx 1$. The projection of internal shear propagators then evaluates to

$$\sigma^*[\mu-\alpha]^{-1}\sigma^* \approx -\left\langle \frac{\Lambda_0^2}{k_s^2}\right\rangle \frac{\left\langle 1-\frac{4}{3}k_{sh}^2/\Lambda^2\right\rangle}{(1-k_{sh}^2/\Lambda^2)}\left\langle \frac{\sigma^*}{2K_-}\right\rangle. \tag{133}$$

Thus, for $\Lambda \approx (8/3)k_s^2$, the internal shear propagator becomes orthogonal to the vertex term it previously enhanced. Meanwhile, the compressional propagator, which becomes large in the slow-wave channel, dominates perturbative corrections. This is roughly equivalent to suppressing all terms in a^A in Eqs. (120)–(122), which then recover the naive poroacoustic form, albeit only over a very protracted range.

IX. CONCLUSIONS AND IMPLICATIONS

The replica formulation of Biot theory constructed above extends much of the technology for handling quenched-random scattering in elasticity to porous media. It provides a general definition of the Biot effective medium based on symmetry, and describes a number of qualitative regions of the RG flow relating those parameters across frequencies. An example has shown another form of scattering-induced dispersion that survives in the inviscid-fluid limit, which may be used as an experimental probe of volume heterogeneity.

A general result from elastic theory—that quenched-random roughness at small scales is RG *relevant*—remains true for Biot theory, though in a more complicated form. The RG has two qualitative regions: wave numbers above and wave numbers below the physically allowed (on-shell) values. Wave numbers above are treated by the real renormalization of scattering vertex coefficients here; the other region must be treated with the methods of localization developed in the companion article.[7] Though *all* fluctuations give rise to scattering loss that is relevant below the on-shell wave number,[3] only density-induced scattering is relevant above. This simplification leads to a tractable set of interactions, in some limits.

The main universal behavior identified here—a flow to strong coupling that isolates the slow wave—appears possible for a range of initial parameters, but not implied for all grain-scale descriptions. It is the generic behavior of an artificial truncation of the theory to compressional excitations only, but in realistic systems must begin from scattering-induced corrections depending on the form of the density matrix. This behavior therefore most likely describes a domain of attraction, being universal within that domain. As in elastic theory, the initial value of the coupling grows as the Rayleigh cross section (as ω^4). Therefore, any qualitative change from classical Biot theory induced by scattering, such as localization of one or more wave component, is expected to occur above a critical frequency.

The asymptotic result of this RG flow is a breakdown of the perturbation theory in which it is defined, and cannot therefore be interpreted directly. Rather, it is interesting because it proposes that some range of initial conditions renormalize to focus scattering enhancements on the slow wave. This gives a limited universal form for the scattering vertex, which can be used as input to a localization calculation equivalent to those performed for acoustic and elastic systems. It further illustrates the fragility of the slow wave under small-scale randomness, not shared by the fast compressional wave to the extent that it has a larger wavelength.

An interesting feature of Biot renormalization not present in classical elasticity is the strong contribution of fluid scattering near the natural scale. It can be interpreted as an inertial entrainment of part of the fluid in the long-wavelength effective solid matrix. Entrainment reduces the effective porosity, averages the bare grain and fluid densities in the effective grain density, and generically increases the shear wave speed. It appears also to increase the fast wave speed in a fairly general class of realistic models. Finally, the interaction terms rendered large under this RG range focus scattering on the fluid-fluid Green's function, which will generally couple more strongly to slow than to fast waves in the longitudinally dominated range that follows.

ACKNOWLEDGMENTS

This work was supported by the Office of Naval Research, Code 321OA, Grant No. N00014-98-1-0118. The author also wishes to acknowledge the helpful suggestions of David Johnson.

APPENDIX A: STABILITY AND NONSTATIONARY SOLUTIONS

The simplest form-preserving, nonstationary evaluation of the compressional RG arises from bare interactions with all σ^α in the plane of $[K_0]$ [defined in Eq. (14)]. Even for this case, when $\xi \neq 0$, Eqs. (62) and (63) do not separate to yield a single value of ξ for all components $\Gamma\alpha\beta$. A formally exact solution of these flow equations may be obtained by letting $\xi \sim 1/d \to 0$. Alternatively, the qualitative features of the flow may be seen by treating Eq. (62) as if there remained an effective ξ, with values asymptotically near the stationary value from Eq. (67). The latter approach will be taken here.

In keeping with the approximate treatment of ξ, parameter groups in Eq. (62) will be replaced with formal parameters

$$\frac{8}{\pi^2}\left(\frac{1}{15}+\frac{2}{15}\xi+\frac{1}{15}\xi^2\right)\to a, \tag{A1}$$

$$\frac{8}{\pi^2}\left(\frac{1}{6}+\frac{11}{15}\xi+\frac{2}{5}\xi^2\right)\to b, \tag{A2}$$

where a and b are expected to remain near the values of Eqs. (A1) and (A2) with $\xi \sim 1/d$ small and positive, and need not be more precisely specified. In the $\sigma_\pm$ basis of Sec. VI B, the flow equations are nondimensionalized by introducing rescaled coupling coefficients

$$\gamma_{++} \equiv \frac{\Gamma_{++}}{K_+^2}\left(\frac{\Lambda}{\Lambda_0}\right)^{4-d}, \tag{A3}$$

$$\gamma_{--} \equiv \frac{\Gamma_{--}}{K_-^2}\left(\frac{\Lambda}{\Lambda_0}\right)^{4-d}, \tag{A4}$$

$$\gamma_{+-} \equiv \frac{\Gamma_{+-}}{K_+ K_-}\left(\frac{\Lambda}{\Lambda_0}\right)^{4-d}, \tag{A5}$$

and recalling that $\Gamma_{-+}=\Gamma_{+-}$. A convenient affine coordinate z is defined differentially from the dimensionless scale factor, as

$$dz \equiv \frac{a+2b}{4-d} d\left(\frac{\Lambda_0}{\Lambda}\right)^{4-d}; \tag{A6}$$

when a and b are constant, this amounts to an overall rescaling.

The flow equation (62) reduces, for the diagonal elements of the coupling, to

$$\frac{d\log\gamma_{++}}{dz} = \gamma_{++} \tag{A7}$$

and

$$\frac{d\log\gamma_{--}}{dz} = \gamma_{--}, \tag{A8}$$

which are integrated directly to produce solutions of the form (69). For the off-diagonal element, the relation is

$$\frac{d\log\gamma_{+-}}{dz} = \frac{a}{a+2b}\gamma_{+-} + \frac{2b}{a+2b}\left(\frac{\gamma_{++}+\gamma_{--}}{2}\right). \tag{A9}$$

γ_{++} and γ_{--}, as autocorrelation coefficients, are necessarily positive. It follows that, for initial $\gamma_{+-}<0$, $|\gamma_{+-}|$ lags γ_{++} and γ_{--}, so while asymptotically $\log(\gamma_{+-})\to\infty$, the flow is driven by the maximum of γ_{++} and γ_{--}. The other case, $\gamma_{+-}\geqslant 0$, will now be shown to have the same asymptotic behavior. The starting point is the elementary triangle inequality

$$\left(\frac{\gamma_{++}+\gamma_{--}}{2}\right) = \sqrt{\gamma_{++}\gamma_{--} + \left(\frac{\gamma_{++}-\gamma_{--}}{2}\right)^2} \geqslant \sqrt{\gamma_{++}\gamma_{--}}, \tag{A10}$$

which, with relations (A7)–(A9) and $\gamma_{+-}\geqslant 0$, implies the bound on the evolution of $\log\gamma_{+-}$

$$\frac{d\log\gamma_{+-}}{dz} = \frac{2b}{a+2b}\left\{1+\frac{a}{2b}\frac{2\gamma_{+-}}{\gamma_{++}+\gamma_{--}}\right\}\frac{d\log\sqrt{\gamma_{++}\gamma_{--}}}{dz} \leqslant \frac{2b}{a+2b}\left\{1+\frac{a}{2b}\frac{\gamma_{+-}}{\sqrt{\gamma_{++}\gamma_{--}}}\right\}\frac{d\log\sqrt{\gamma_{++}\gamma_{--}}}{dz}, \tag{A11}$$

with equality only in the degenerate case $\gamma_{++}=\gamma_{--}$. The ratio in the bounding equation in Eq. (A11) also has a bounded flow equation:

$$\frac{d\log(\gamma_{+-}/\sqrt{\gamma_{++}\gamma_{--}})}{dz} = \frac{a}{a+2b}\left\{\gamma_{+-} - \left(\frac{\gamma_{++}+\gamma_{--}}{2}\right)\right\} \leqslant \frac{a}{a+2b}\{\gamma_{+-} - \sqrt{\gamma_{++}\gamma_{--}}\}. \tag{A12}$$

The requirement that, for physical correlation functions, $\Gamma_{+-}^2 \leqslant \Gamma_{++}\Gamma_{--} \Rightarrow \gamma_{+-} \leqslant \sqrt{\gamma_{++}\gamma_{--}}$ as initial conditions, is preserved by Eq. (A12). Any initial difference among γ_{++}, γ_{--}, and γ_{+-} results in an amplified logarithmic derivative strictly less than zero, so that $\gamma_{+-}/\sqrt{\gamma_{++}\gamma_{--}}\to 0$. It then follows from Eq. (A11) that asymptotically

$$\gamma_{+-} \propto (\gamma_{++}\gamma_{--})^{b/(a+2b)}. \tag{A13}$$

None of these conclusions is sensitive to the particular values of a or b, or how these arise from different true ξ values in different graphs, so they should represent the exact case of in-plane initial conditions. The important result is that, except for the highly degenerate case $\gamma_{++}=\gamma_{--}=\gamma_{+-}$, the off-diagonal elements always grow as a power <0.5 of the larger of the diagonal elements, so the evolution is always toward the stationary rays of Sec. VI B. Further, degeneracy of γ_{++} and γ_{--} divides the basins of attraction of the basis rays of $[K_0]$. The condition that flow be toward σ_- is that $G_{++}\leqslant G_{--}(K_+^2/K_-^2)$, which for the parameters quoted above is effectively the whole fluctuation domain.

[1] K. G. Wilson and J. Kogut, Phys. Rep., Phys. Lett. **12C**, 101 (1974).
[2] P. W. Anderson, Phys. Rev. **109**, 1492 (1968); S. He and J. Maynard, Phys. Rev. Lett. **57**, 3171 (1986); G. Papanicolaou, Doc. Math. J. DMV, Extra Volume ICM **1998**, 1 (1998).
[3] S. John, H. Sompolinsky, and M. J. Stephen, Phys. Rev. B **27**, 5592 (1983).
[4] E. Smith, Phys. Rev. B **58**, 5346 (1998).
[5] M. A. Biot, J. Acoust. Soc. Am. **28**, 168 (1956); **28**, 179 (1956).
[6] M. A. Biot, J. Acoust. Soc. Am. **34**, 1254 (1962).
[7] E. Smith, following paper, Phys. Rev. B **64**, 134203 (2001).
[8] S. Weinberg, Physica A **96**, 327 (1979).
[9] R. Burridge and J. B. Keller, J. Acoust. Soc. Am. **70**, 1140 (1981).
[10] M. A. Biot and D. G. Willis, J. Appl. Mech. **24**, 594 (1957).
[11] J. L. Auriault, J. Acoust. Soc. Am. **77**, 1641 (1985); Arch. Mech. **40**, 529 (1988).
[12] S. R. Pride, A. F. Gangi, and F. D. Morgan, J. Acoust. Soc. Am. **92**, 3278 (1992).

[13] J. G. Cardy, J. Phys. C **11**, L320 (1978).
[14] D. L. Johnson, D. L. Hemmick, and H. Kojima, J. Appl. Phys. **76**, 104 (1994).
[15] D. L. Johnson, J. Koplik, and R. Dashen, J. Fluid Mech. **176**, 379 (1987).
[16] R. D. Stoll, *Sediment Acoustics* (Springer-Verlag, New York, 1989), pp. 7–11.
[17] M. D. Collins, J. F. Lingevitch, and W. L. Siegmann, Wave Motion **25**, 265 (1997).
[18] R. D. Stoll and T.-K. Kan, J. Acoust. Soc. Am. **70**, 149 (1981).
[19] D. L. Johnson and T. J. Plona, J. Acoust. Soc. Am. **72**, 556 (1982).
[20] D. L. Johnson, T. J. Plona, and H. Kojima, J. Appl. Phys. **76**, 115 (1994).
[21] The sign of w is used in two different ways in current literature. The convention followed here is that of Refs. 18, 31, and 16. The opposite sign is used in Refs. 6 and 12, and Gurevich and Schoenberg in Ref. 22.
[22] H. Deresiewicz and R. Skalak, Bull. Seismol. Soc. Am. **53**, 783 (1963); J. G. Berryman and L. Thigpen, J. Appl. Mech. **52**, 345 (1985); B. Gurevich and M. Schoenberg, J. Acoust. Soc. Am. **105**, 2585 (1999).
[23] R. Burridge and C. A. Vargas, Geophys. J. R. Astron. Soc. **58**, 69 (1979).
[24] A. N. Norris, J. Acoust. Soc. Am. **77**, 2012 (1985).
[25] G. Bonnet, J. Acoust. Soc. Am. **82**, 1758 (1987).
[26] V. D. Kupradze, T. G. Gezelia, M. O. Basheleishvili, and T. V. Burchuladze, *Three-Dimensional Problems of the Mathematical Theory of Elasticity and Thermoelasticity* (North-Holland, Amsterdam, 1979).
[27] K. H. Fischer and J. A. Hertz, *Spin Glasses* (Cambridge University Press, Cambridge, England, 1993), p. 28.
[28] A. Weinrib and B. I. Halperin, Phys. Rev. B **27**, 413 (1983).
[29] J. Polchinski, Nucl. Phys. B **231**, 269 (1984).
[30] This name is drawn from the identically-structured spacetime of $(2+1)$-dimensional special relativity. Positive-determinant matrices correspond to ''timelike,'' and negative-determinant matrices to ''spacelike'' vectors, and null, or zero-determinant matrices, form cones of ''lightlike'' vectors.
[31] M. Stern, A. Bedford, and H. R. Millwater, J. Acoust. Soc. Am. **77**, 1781 (1985); N. P. Chotiros, *ibid.* **97**, 199 (1995).
[32] J. G. Berryman, J. Math. Phys. **26**, 1408 (1985); C. Zimmerman and M. Stern, J. Acoust. Soc. Am. **94**, 527 (1993).
[33] N. P. Chotiros, J. Acoust. Soc. Am. **103**, 2726 (1998).
[34] J. Heiserman, J. P. Hulin, J. Maynard, and I. Rudnick, Phys. Rev. B **14**, 3862 (1976).
[35] J. G. Berryman, J. Acoust. Soc. Am. **69**, 416 (1981).